

Review article

Seied Ali Safiabadi Tali and Wei Zhou*

Multiresonant plasmonics with spatial mode overlap: overview and outlook

<https://doi.org/10.1515/nanoph-2019-0088>

Received March 22, 2019; revised June 11, 2019; accepted June 18, 2019

Abstract: Plasmonic nanostructures can concentrate light and enhance light-matter interactions in the subwavelength domain, which is useful for photodetection, light emission, optical biosensing, and spectroscopy. However, conventional plasmonic devices and systems are typically optimized for the operation in a single wavelength band and thus are not suitable for multiband nanophotonics applications that either prefer nanoplasmonic enhancement of multiphoton processes in a quantum system at multiple resonant wavelengths or require wavelength-multiplexed operations at nanoscale. To overcome the limitations of “single-resonant plasmonics,” we need to develop the strategies to achieve “multiresonant plasmonics” for nanoplasmonic enhancement of light-matter interactions at the same locations in multiple wavelength bands. In this review, we summarize the recent advances in the study of the multiresonant plasmonic systems with spatial mode overlap. In particular, we explain and emphasize the method of “plasmonic mode hybridization” as a general strategy to design and build multiresonant plasmonic systems with spatial mode overlap. By closely assembling multiple plasmonic building blocks into a composite plasmonic system, multiple nonorthogonal elementary plasmonic modes with spectral and spatial mode overlap can strongly couple with each other to form multiple spatially overlapping new hybridized modes at different resonant energies. Multiresonant plasmonic systems can be generally categorized into three types according to the localization characteristics of elementary modes before mode hybridization, and can be based on the optical coupling between: (1) two or more localized modes, (2) localized

and delocalized modes, and (3) two or more delocalized modes. Finally, this review provides a discussion about how multiresonant plasmonics with spatial mode overlap can play a unique and significant role in some current and potential applications, such as (1) multiphoton nonlinear optical and upconversion luminescence nanodevices by enabling a simultaneous enhancement of optical excitation and radiation processes at multiple different wavelengths and (2) multiband multimodal optical nanodevices by achieving wavelength multiplexed optical multimodalities at a nanoscale footprint.

Keywords: multiresonant plasmonics; mode hybridization; spatial mode overlap; nonlinear plasmonics; wavelength-multiplexed multimodal plasmonics.

1 Introduction

Plasmonic devices and systems based on bottom-up synthesized or top-down fabricated metal nanostructures can be used to enhance light-matter interactions at nanoscale in physical, chemical, and biological systems [1–19]. For example, plasmonic nanocavities and nanoantennas have shown unique capabilities for ultrasensitive detection and analysis of chemical and biological species [8–10], collection and concentration of light in nanoscale optoelectronics and nonlinear optics devices [2–7], localized photothermal intervention of cells or cellular networks [11–15], and optical generation of hot carriers in photocatalytic processes [16–19]. For some of the directions being pursued with plasmonic nanostructures, such as the spontaneous down-conversion photoluminescence and refractive index based nanooptics sensing, single-resonant enhancement of light-matter interactions in one wavelength range is sufficient. Nevertheless, there are applications that prefer a multiresonant plasmonic enhancement of light-matter interactions at nanoscale in multiple wavelength ranges (Figure 1) such as those benefiting from a simultaneous enhancement of both excitation

*Corresponding author: Wei Zhou, Department of Electrical and Computer Engineering, Virginia Tech, Blacksburg, VA 24060, USA, e-mail: wzh@vt.edu. <https://orcid.org/0000-0002-5257-3885>

Seied Ali Safiabadi Tali: Department of Electrical and Computer Engineering, Virginia Tech, Blacksburg, VA 24060, USA

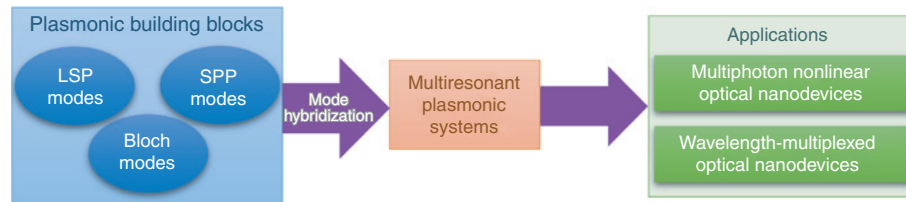


Figure 1: A block-diagram illustration of the strategy to create multiresonant plasmonic systems by plasmonic mode hybridization and the potential applications enabled by multiresonant plasmonics with spatial mode overlap.

By the optical coupling between elementary modes (e.g. LSP modes, SPP modes, and Bloch modes) in different types of plasmonic building blocks, it is possible to design and create “multiresonant plasmonic systems with spatial mode overlap” that can support multiple plasmonic modes with strong local field enhancements at same locations in multiple different wavelength ranges. Potential applications regarding multiresonant plasmonics include (1) multiphoton nonlinear optical nanodevices that can enhance both excitation and emission rates in multiphoton nonlinear processes or in multiphoton upconversion luminescence processes and (2) wavelength-multiplexed optical nanodevices that can achieve multimodal optical operations at nanoscale using multiple spectral bands.

and emission rates in multiphoton parametric nonlinear processes [20–31] as well as in multiphoton upconversion (UC) luminescence processes [32–34], or those requiring wavelength-multiplexed multimodal operations at nanoscale [35–37]. To address such multiband nanophotonics applications, we need to go beyond the conventional single-resonant plasmonics and advance to multiresonant plasmonic systems. On the basis of the mode hybridization strategy [38, 39], it is possible to create multiresonant plasmonic systems based on closely assembled plasmonic building blocks, in which the associated elementary modes in the building blocks can strongly interact to form multiple new hybridized plasmonic modes at different wavelengths with spatial mode overlap. We refer to this type of plasmonic systems as “multiresonant plasmonic systems with spatial mode overlap” (Figure 1), which are able to achieve nanoscale enhancement of light-matter interactions in multiple different wavelength ranges at the same locations.

In this review, we aim to present an overview of the theoretical background and experimental demonstrations of “multiresonant plasmonic systems with spatial mode overlap” and discuss the implications and opportunities in this research direction. The manuscript is organized as follows: Section 2 summarizes the basic concepts related to the different types of localized and delocalized plasmonic modes, the mode hybridization theory, and geometrical symmetry effects. In Section 3, we will introduce three general strategies for the design and creation of multiresonant plasmonic systems with spatial mode overlap by exploiting optical coupling between (1) two or more localized modes, (2) localized and delocalized modes, and (3) two or more delocalized modes in different types of plasmonic building blocks. Finally, Section 4 is dedicated to the discussion of current and potential applications that can benefit from the multiresonant enhancement of

local optical fields in multiple wavelength ranges at the same locations.

2 Fundamental concepts

By closely assembling several plasmonic building blocks into a composite plasmonic system, it is possible for their associated elementary plasmonic modes to strongly interact with each other and thus generate multiple new hybridized modes at different resonant wavelengths with spatial mode overlap. In this section, we briefly review the physics governing elementary surface plasmon modes in different types of plasmonic building blocks and their optical interactions. We begin by a short explanation of elementary plasmonic modes in the several types of basic building blocks, including propagating surface plasmon polariton (SPP) modes at extended continuous metal-dielectric interfaces, localized surface plasmon (LSP) modes at confined nanoscale metal-dielectric interfaces, and delocalized Bloch plasmonic modes (or lattice plasmon modes) in periodic metal-dielectric nanostructures. Then, we give a brief discussion of plasmonic mode hybridization. Finally, we explain the effects of the geometrical symmetry on the optical properties of plasmonic systems.

2.1 Propagating SPP modes at continuous metal-dielectric interface

SPPs are evanescent electromagnetic surface waves propagating at an extended continuous metal-dielectric interface where the real part of the dielectric function changes sign [40]. The simplest structure that can sustain SPP waves is a single and flat interface between a lossless dielectric half-space and a metal half-space (Figure 2A).

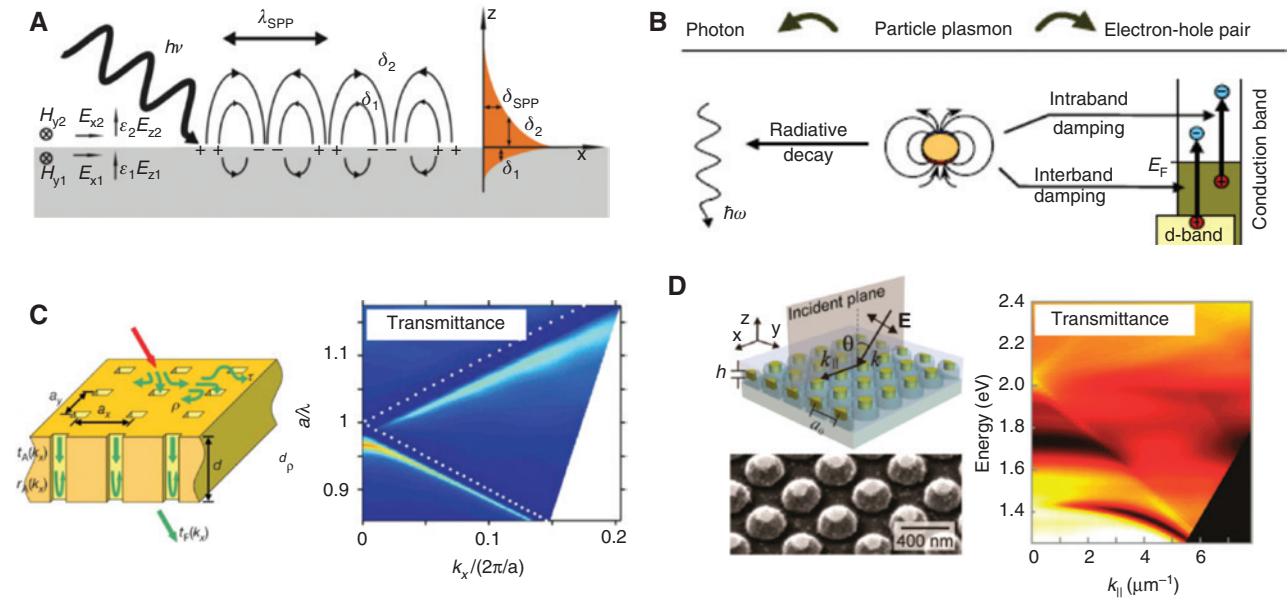


Figure 2: Schematic illustrations of plasmonic modes in different types of plasmonic building blocks.

(A) Surface plasmon polariton (SPP) modes at the continuous metal-dielectric interfaces. (B) Localized surface plasmon (LSP) modes in individual metal nanostructures [41]. (C) Delocalized Bloch-SPP modes in the metal thin film perforated with periodic nanohole arrays [42]. (D) Delocalized out-of-plane lattice plasmon modes in Au nanoparticle arrays [43].

In such case, only transverse magnetic (TM) SPPs are allowed [44], and the SPP dispersion relation is as follows:

$$\beta = k_0 \sqrt{\frac{\epsilon_d \epsilon_m}{\epsilon_d + \epsilon_m}}, \quad (1)$$

where β is the SPP wavenumber, k_0 is the free space wave-number, ϵ_d is the dielectric relative permittivity, and ϵ_m is the metal dielectric function. As revealed by Equation 1, SPPs carry larger momentums than free-space photons and thus can achieve the subwavelength confinement of optical fields beyond the diffraction limit. However, for optical excitation of SPPs, we need to bridge this momentum mismatch between photons in the free-space and SPPs at planar metal-dielectrics interface using methods such as prism coupling, grating coupling, and near-field coupling by nanostructured geometries [44, 45]. As there are both radiative and nonradiative losses for SPPs propagating at the metal-dielectric interface, the wavevector of SPP modes is a complex number. While the radiative losses of SPPs are mainly associated with the scattering by nanoscale surface roughness, their nonradiative losses mostly originate from the intraband and the interband damping of the SPP-excited conduction band electrons in the metal. In general, the dispersion properties of SPPs can be engineered either by choosing different metal and dielectric materials (and thus their optical constants) or by the optical hybridization with other plasmonic modes

in the neighboring building blocks (more discussion will be given in the Subsection 2.4).

2.2 LSP modes in individual metal nanostructures

LSPs are associated with the collective oscillations of conduction band electrons in coupling with surface EM fields in confined nanoscale metal-dielectric interfaces (Figure 2B) [41, 46]. This confinement, which can be three-dimensional (3D) as in nanoparticles or nanovoids or two-dimensional in the case of nanowires or nanogrooves, causes charge accumulations of opposite signs on metallic surfaces. This leads to the formation of amplified electric fields in the nanostructure near-field zone. Similarly, induced electric oscillation currents can induce localized magnetic fields at plasmonic nanostructures. Intuitively, LSPs can be considered as standing wave SPP modes at metal-dielectric interfaces in confined nanostructures, and therefore, it is possible for the same metal-dielectric nanostructures to support multiple LSP modes with different (standing wave) orders at different wavelengths in optical wavelength range. However, high-order LSP modes typically have a dark multipolar nature and thus cannot interact with free-space light effectively [47, 48]. In contrast, the lowest-order LSP mode (in analogy with the ground state in a quantum system) has an electric dipolar

nature and thus can effectively interact with the free-space light in both excitation and scattering processes. Compared with SPPs, LSPs can induce much more concentrated charge accumulations because of the nanoscale geometric confinement, which results in larger amplitude of oscillating electric currents, larger near-field enhancement factors for both electric and magnetic fields, and larger nonradiative damping rates (or lower resonant quality factors). LSPs can decay through radiative channels (scattering) by conversion to photons and nonradiative channels (absorption) because of the creation of electron-hole pairs (Figure 2B) [41]. As the simplest nanoplasmonic system, a subwavelength metallic nanosphere can support the electrical dipolar LSP mode [44] with the scattering cross section (C_{sca}) and the absorption cross section (C_{abs}) expressed as follows:

$$C_{\text{sca}} = \frac{8\pi}{3} k_0^4 a^6 \left| \frac{\epsilon_m - \epsilon_d}{\epsilon_m + 2\epsilon_d} \right|^2, \quad (2)$$

$$C_{\text{abs}} = 4\pi k_0 a^3 \text{Im} \left[\frac{\epsilon_m - \epsilon_d}{\epsilon_m + 2\epsilon_d} \right], \quad (3)$$

where k_0 is the free space wavenumber, a is the sphere radius, ϵ_d is the dielectric relative permittivity, and ϵ_m is the metal dielectric function. From these two equations, we can see that while radiative decay is the major loss mechanism for LSPs in larger nanoparticles, nonradiative decay dominates for smaller nanoparticles. By tailoring the geometries (e.g. size and shape), materials at nanoscale metal-dielectric interface, and optical interactions with other plasmonic modes, it is possible to control both far-field and near-field characteristics of LSPs.

2.3 Delocalized Bloch plasmonic modes in periodic metal-dielectric nanostructures

Periodic dielectric structures called photonic crystals can support Bloch photonic modes, which can be considered as the electromagnetic analogue of Bloch electron waves in the periodic atomic crystals [49]. Similarly, periodic metal-dielectric nanostructures can support Bloch plasmonic modes delocalized over the whole lattice system under the Bloch boundary condition. Compared with Bloch photonic modes in a dielectric system, Bloch plasmonic modes can induce much higher local optical field enhancement factors as well as larger optical losses as a result of the collective coupling between surface EM waves in the dielectric medium and surface charge density

waves in the metal nanostructures [50]. On the basis of the Bloch theorem [49], the electric and magnetic field of a Bloch plasmonic mode can be expressed in the form of $\mathbf{E}/\mathbf{H}_k(\mathbf{r}) = e^{i\vec{k}\cdot\vec{r}} \mathbf{u}_k(\mathbf{r})$, where \vec{k} is the Bloch wavevector and $\mathbf{u}_k(\mathbf{r})$ is the periodic envelope function with the periodicity of the lattice constant. Analogous to Bloch photonic modes in photonic crystals, Bloch plasmonic modes in periodic metal-dielectric nanostructures can exhibit dispersive band structures that determine the dependence of its mode resonant energy on its wavevector (momentum) [51] (Figure 2C and D). Therefore, the optical properties of periodic metal-dielectric nanostructures, which can support not only localized plasmonic modes but also delocalized Bloch plasmonic modes, can be very different from their individual unit cells, which only support localized plasmonic modes.

Periodic metal-dielectric nanostructures can be constructed in a large variety of designs with many degrees of freedom in choosing geometry and material parameters. However, depending on geometric continuity of the metal-dielectric interface across the boundary of unit cells, there are two basic types of periodic metal-dielectric nanostructures: (1) periodically modulated continuous metal surfaces, and (2) periodic arrays of discretized metal nanostructures.

Periodically modulated continuous metal surfaces, such as one-dimensional (1D)/two-dimensional (2D) opaque metal gratings and metal thin films perforated with periodic arrays of nanoholes (Figure 2C), can support the so-called SPP-Bloch modes at the continuous metal-dielectric interface. By adding the grating momentum to bridge the momentum mismatch between photons and SPP-Bloch modes, the excitation condition of SPP-Bloch modes in a periodic structure can be described by the Bragg coupling equation $\vec{k}_{\parallel} + \vec{G} = \vec{k}$, where \vec{G} is a reciprocal lattice vector and \vec{k}_{\parallel} is the in-plane wave vector of the incident light [51]. In the past two decades, numerous experimental and theoretical studies on the optical properties of the periodic nanohole arrays in the opaque metal film have revealed that the excitation of Bloch-SPP modes on both sides of the metal film can mediate the extraordinary optical transmission process observed in such system [42, 51, 52].

Unlike periodically modulated continuous metal surfaces, periodic arrays of discretized metal nanostructures with a large dielectric spacing, such as 1D arrays of metal nanowires and 2D arrays of metal nanoparticles (Figure 2D), do not support SPP-Bloch modes because of the large deviation from the continuous metal-dielectric interface boundary conditions of the unit cell. Instead, they can support collective lattice plasmon modes mediated

by the diffractive coupling between LSP modes in individual metal nanostructures [53]. In an intuitive picture, the lattice plasmon modes in periodic metal nanoparticle array can be induced when the grating order is changed from radiative to evanescent so that the optical energy scattered by one nanoparticle can be collected by neighboring nanoparticles as collective lattice plasmons instead of decaying as free-space light [54–56]. Coupled dipole theory has predicted that strongly coupled nanoparticles in one-dimensional arrays can produce extremely narrow lattice plasmon resonances by suppressing radiative loss [57]. Experiments have reported that two polarization types of lattice plasmon resonances can exist in two-dimensional arrays of gold and silver nanoparticles: (1) the in-plane lattice plasmon modes mediated by in-plane dipolar interactions between unit cells [58–61] and (2) the out-of-plane lattice plasmon modes mediated by out-of-plane dipolar interactions between unit cells [43, 56]. From the framework of Bloch theorem, lattice plasmon modes can be considered as a type of surface Bloch mode composed of many Bloch harmonics in periodic arrays of discretized metal nanostructures and also can exist in transverse electric polarization mode mediated by in-plane dipolar interactions as well as TM polarization mode mediated by out-of-plane dipolar interactions. A recent study has shown that out-of-plane lattice plasmon modes in 2D Au nanoparticle arrays exhibit dispersive quality factors associated with the highly dispersive nature of such TM Bloch mode [43]. As the dispersion curve of the out-of-plane lattice plasmon modes evolves from a stationary state to a propagating state, the nonradiative loss decreases because of weak local field confinement, whereas the radiative loss increases because of strong coupling to the leaky zero-order Bloch harmonic component [43].

2.4 Mode hybridization

The previous sections have introduced SPPs, LSPs, and Bloch lattice plasmons as elementary plasmonic modes supported in different types of building blocks. By putting two plasmonic building blocks very close to each other, their elementary modes with similar resonant energies can exert EM forces and exchange EM energy with each other through very intense near-field EM interactions. In such situation, we call these two elementary plasmonic modes “coupled” with each other, and two new “hybridized” modes form at modified resonant wavelengths that have mutually mixed far-field and near-field optical characteristics. In order to achieve a strong coupling between modes, three conditions need to be satisfied for the

participating elementary modes: (1) spectral overlap of mode resonant energies, (2) spatial overlap of mode profiles, and (3) the nonorthogonality between the modes.

If we model the interacting plasmonic modes as mechanical oscillators with attenuation coefficients γ_1 and γ_2 (Figure 3A), the coupling strength (g) between the two modes can be treated as the constant of spring connecting the two oscillators [62, 68, 69]. Therefore, the coupling strength between the two plasmonic modes determines the energy exchange rate between them. As illustrated in the phase diagram in Figure 3B, depending on the relative values of the decay constants of each mode (γ_1 and γ_2) with regard to the coupling strength (g), the interaction between the two plasmonic modes can be in the weak coupling regime (when $|g| \ll |\gamma_1|$, or $|\gamma_2|$) or in the strong coupling regime (when $|g| \gg |\gamma_1|$, and $|\gamma_2|$). Some important phenomena in the weak coupling regime include Fano resonance [62, 68–71] (red region), electromagnetically induced transparency [62, 72–74] (red region), and Kerker effect [62, 75–77] (red and white regions). Fano resonance shows an asymmetric spectral line-shape with a sharp change between a dip and a peak. Microscopically, it arises due to the constructive-destructive interference between a narrow-linewidth discrete mode (such as dark high-order plasmonic modes and diffraction lattice plasmon modes) and a broad-linewidth mode (such as an electric dipole mode or a background continuum) [78]. In the model of two coupled oscillators, Fano resonance happens when only one of the oscillators (the one with the larger damping) is driven by the external force [62]. Electromagnetically induced transparency can be considered as a special case of Fano resonance in which, the two oscillators have the same resonance frequency [62]. Kerker effect is the directional scattering due to the interference of the electric and magnetic dipole modes' independent responses to the external field in the limit of vanishing direct coupling. In this case, both oscillators are driven, and the damping rate ratios can be arbitrary [62]. In the strong coupling regime (blue region in Figure 3B), the energy exchange rate between the two coupled oscillators is much larger than the energy leaking rates, and thus, two new hybridized eigenmodes can form with their resonance frequencies shifted away from those of the original uncoupled modes. The modification of eigen-energies, which are associated with the new hybridized eigenmodes of different charge distribution profiles, is called “Rabi splitting” or “Autler-Townes splitting” (Figure 3C) [62, 63, 67, 74]. As expected, the amount of energy splitting between new hybridized modes strongly depends on the amount of spatial mode overlap between interacting fundamental modes in the plasmonic building blocks [63]. So far,

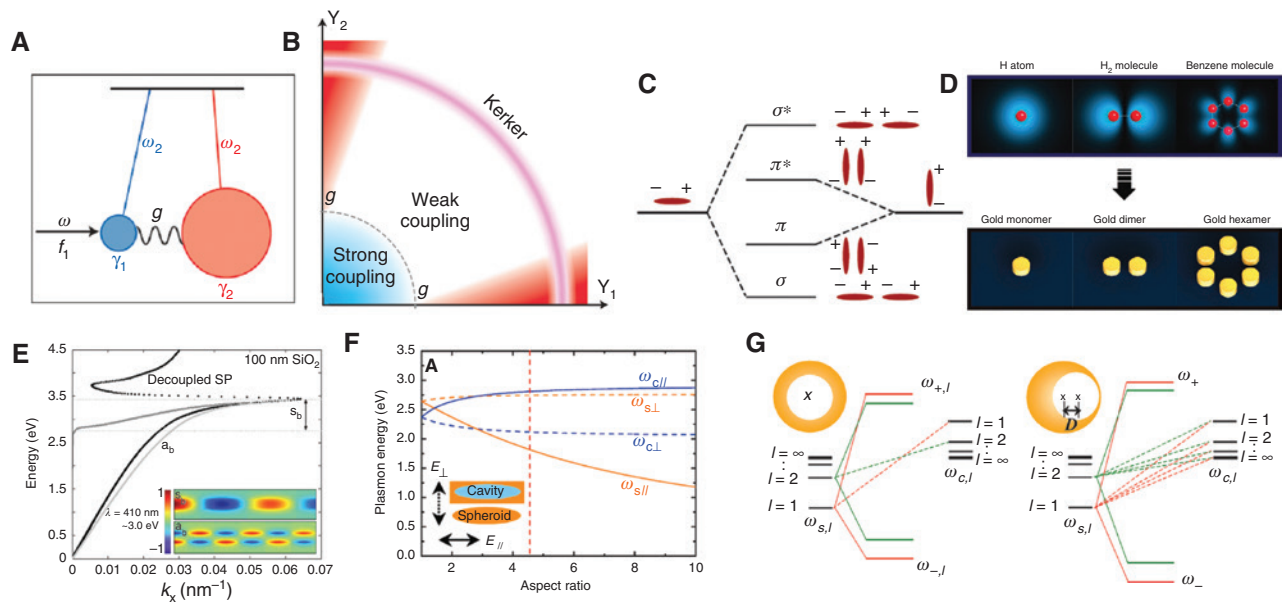


Figure 3: Plasmonic mode hybridization basics.

(A) Schematic illustration of two coupled oscillators with the coupling strength g and individual damping coefficients γ_1 and γ_2 [62]. (B) Phase diagram showing the separation between the weak coupling regime ($g \ll \gamma_1, \gamma_2$) and the strong coupling regime ($g \gg \gamma_1, \gamma_2$) [62]. (C) Energy diagram showing the Rabi splitting for two strongly coupled electric dipolar LSP modes in σ and π configurations [63]. (D) Schematic illustration of the analogy between the plasmonic mode hybridization and molecular orbital hybridization [64]. (E) Dispersion curves for the symmetric and antisymmetric modes of a MIM slot waveguide based on silver and SiO₂ (100 nm thickness) [65]. The inset shows the E_x profiles at $\lambda = 410$ nm. (F) Plasmon energy vs. aspect ratio for the solid prolate spheroid and the prolate cavity systems. The solid and dashed lines represent longitudinal and transverse polarizations, respectively [66]. (G) The energy diagrams regarding LSP hybridization in concentric (left) and nonconcentric (right) nanoshells [67].

several types of numerical and analytical methods have been developed to analyze the plasmon coupling effect [38, 39, 79–90]. Introduced by Peter Nordlander’s group as an electromagnetic analog of the molecular orbital hybridization theory [38, 39], the method of “plasmon hybridization” can provide an intuitive microscopic picture to treat the plasmonic modes in composite plasmonic nanostructures as the hybridized modes from the elementary modes in its plasmonic building blocks [64, 91] (Figure 3C and D).

On the basis of the localization nature of the elementary modes in the building blocks, there are three general scenarios to form new hybridized modes in a composite plasmonic system: (1) from the coupling between two or more localized plasmonic modes; (2) from the coupling between two or more delocalized plasmonic modes; and (3) from the coupling between localized and delocalized plasmonic modes. For example, the elementary SPP modes at the multiple interfaces in metal-insulator-metal (MIM) composite thin films can interact with each other to form multiple hybridized SPP modes, whose dispersion curves will shift away from those of their elementary modes (Figure 3E) [44, 65, 92–95]. The inset of Figure 3E depicts the mode profiles of two hybridized SPP modes,

respectively, with symmetric and antisymmetric distribution of their field components [65].

2.5 Effects of geometrical symmetry

An object can have a symmetry when there is a geometrical transformation under which it is mapped to itself. Also, it is called to have an antisymmetry if the object only change sign upon a transformation [96]. In general, when the geometry of a plasmonic system is symmetric under a specific geometrical transformation, its modes can be defined such that all of their components (electric field, magnetic field, and charge and current distribution) are either symmetric or antisymmetric with respect to the same transformation [97].

By reducing the geometrical symmetry of a composite plasmonic system that consists of multiple building blocks, it is possible to modify the optical characteristics of supported modes and then improve the multiresonant optical response of the system via the following effects: (1) lifting-off the energy degeneracy of the supported modes [66, 97] (Figure 3F), (2) increasing the nonorthogonality

between the elementary modes for an effective mode hybridization [67] (Figure 3G), and (3) increasing the radiative decay rates of the supported dark modes for optical excitation under the free-space light illumination [97]. The first scenario can happen when the high symmetry in the initial plasmonic system results in some degenerated modes at the same resonant energy with identical field profiles (as well as charge distributions) but with different polarization directions. The second scenario can happen when some elementary modes in the building blocks are initially orthogonal to each other and thus cannot interact with each other despite having spatial and spectral overlap. The last scenario can occur when the plasmonic mode initially have an opposite symmetry of fields with the incident free-space light.

2.6 How to build multiresonant plasmonic systems with spatial mode overlap?

On the basis of the above discussions, we can generate several guidelines for the design and creation of a composite plasmonic system that can support multiple hybridized plasmonic modes with spatial mode overlap. First, the composite system should be carefully designed using building blocks that support elementary modes with similar resonant energies to have the required spectral mode overlap for a further effective mode hybridization. Second, the building blocks of the composite plasmonic system should be closely packed to each other so that the elementary modes can spatially overlap and hybridize. For non-orthogonal modes, the higher this spatial mode overlap is, the higher the hybridization strength will be. Third, the symmetry of the composite plasmonic system can be reduced in order to lift-off the energy degeneracy of supported modes and allow a higher nonorthogonality between elementary modes for their effective hybridization. Finally, the symmetry and the orientation arrangement between the composite plasmonic system and incident free-space light should be carefully considered so that the supported modes in the system are not so dark to prevent an effective interaction with the free-space light. This can be done either by making their net electric or magnetic dipole moments nonzero (via nonsymmetric geometry design for high order modes) so as to induce an electric/magnetic field component in the direction of their net electric/magnetic dipole, by a near-field coupling with a bright plasmonic mode, or by introducing the phase retardation. In this section, we review how to achieve multiresonant plasmonic systems through the optical coupling between elementary modes in their plasmonic

building blocks. By considering the localization nature of the elementary modes before hybridization, we can broadly categorize into three basic types of multiresonant plasmonic systems on the basis of the optical coupling between (1) two or more localized modes, (2) localized and delocalized modes, and (3) two or more delocalized modes. More complex designs by combining two or all of these strategies are also possible.

2.7 Coupling between two or more localized plasmonic modes

In multiresonant plasmonic systems based on the optical coupling between two or more localized modes, the building blocks are closely located metal nanostructures that support LSPs as elementary modes for mode hybridization. According to the arrangement of the nanoparticle building blocks, the multiresonant systems using the localized-localized mode coupling strategy can be classified into three subgroups: (1) in-plane composite nanostructures, (2) core-shell composite nanostructures, and (3) out-of-plane composite nanostructures.

2.7.1 In-plane composite nanostructures

In-plane composite nanostructures consist of metallic nanoparticles or nanovoids (continuous void pieces carved in metallic films) as the plasmonic building blocks in a planar arrangement close to each other. In-plane composite nanostructures can be classified in terms of the number of the nanoparticles or nanovoids that form them. A structure that is composed of n nanoparticles (or nanovoids) is called a n -mer (usually read in the Greek system) nanostructure. In this regard, these structures are also generally called “metallic oligomer clusters.” Several types of in-plane composite plasmonic nanostructures with various number, shape, and arrangement of the nanoparticles have so far been reported in the literature. Monomers are the simplest type of in-plane nanostructures. They consist of only one metallic nanoparticle (or nanovoid) that can support several plasmonic modes depending on their geometric symmetry. In more complex oligomers (dimer and above), the LSP modes related to adjacent nanoparticles (or nanovoids) can hybridize with each other through near-field optical interactions. Properties of the hybridized modes depend on the nature of the individual building block modes, the number of nanoparticles or nanovoids, and their arrangement with respect to each other. In-plane composite plasmonic

systems typically can support multiple in-plane modes with a net in-plane polarization. As the current distributions related to in-plane modes are also in-plane, their associated magnetic multipole moments are out-of-plane and typically cannot be excited by the in-plane magnetic field component of the normally incident light. Moreover, as there is no phase retardation between light and different in-plane building blocks under the normal light excitation condition, these in-plane modes can be excited by the electric field only if they have a nonzero net electric dipole moment. Without an optimized design to reduce the geometrical symmetry of the in-plane oligomer systems, in-plane multipolar high-order modes can be very dark and thus can hardly be observed from the far-field optical measurements [97–111]. Here we first examine monomer, dimer, and trimer cases and then, discuss higher-order oligomer systems.

There exist several examples in the literature in which monomer systems are reported to display multiresonant behaviors [34, 112–114]. Yet, because of the following reasons, they are not generally considered to be appropriate for the tasks that require a multiresonant response under the free-space light excitation. First, symmetries in the system can make most high-order multipolar modes very dark under the normal incident light. Second, resonant wavelengths of individual modes cannot be tuned independently by geometric engineering because of their standing wave-like nature. Finally, without a tight optical field confinement in the MIM nanogaps, the field enhancement of modes in plasmonic monomer nanostructures is usually much smaller compared with plasmon modes in MIM nanogaps.

When two plasmonic monomers get close to each other, they can form plasmonic dimer nanostructures. By introducing MIM nanogaps between two monomers, new hybridized bonding mode can be supported as a type of gap plasmon modes with very large enhancements of both electric fields (also sometimes magnetic fields) inside the MIM nanogap [23, 39, 102–106, 115–127]. Upon proper design, dimer structures can achieve multiresonant response with spatial mode overlap [23, 105, 106, 116–120, 122, 123, 125–127]. Figure 4A illustrates an example of such systems. This nonsymmetric heterodimer consists of a V-shaped gold antenna with an arm length of 180 nm coupled to a 125 nm nanorod-shaped gold nanoantenna through a gap of ~17 nm. The width and thickness of the V-shaped nanoantenna and the nanorod are 30 and 40 nm, respectively [23]. As can be seen from the scattering spectra, the composite dimmer plasmonic nanoantenna can support three major plasmonic modes at 780 (V_2^A), 910 (V_2^B) and 1560 nm (V_1); modes V_2^A and V_2^B

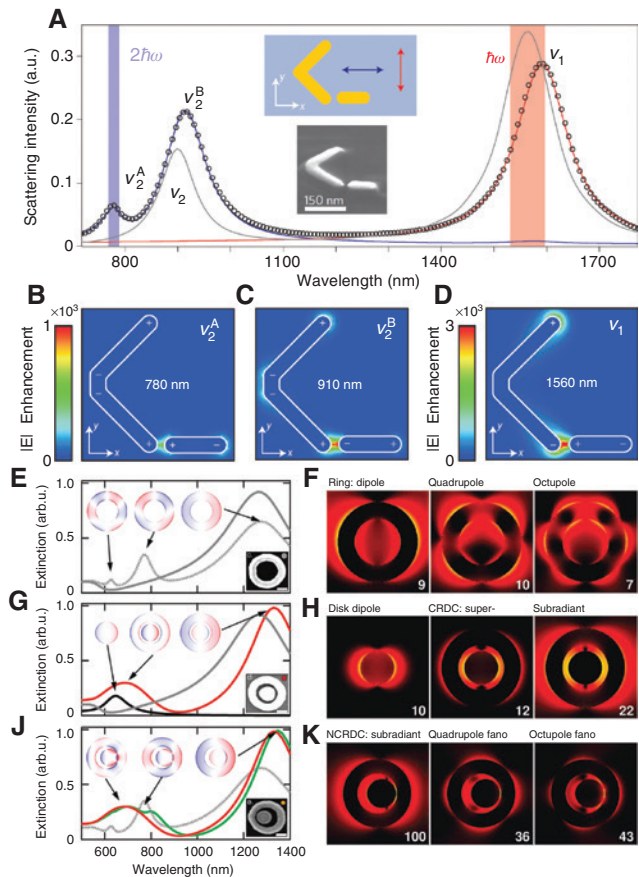


Figure 4: Two examples of multiresonant plasmonic systems based on the optical coupling between localized plasmonic modes in in-plane dimer nanostructures. (A) A plasmonic dimer structure and its far-field scattering spectra [23]. (B–D) The near-field distribution maps of electric field intensity enhancement at its three different resonant wavelengths [23]. (E, G, J) Charge plots and extinction cross sections for cavities formed by different combinations of a disk with $D_{\text{disk}} = 150$ nm and a ring with $D_{\text{out}} = 350$ nm and $D_{\text{in}} = 200$ nm. Legends: ring (solid dark gray), disk (black), symmetric ring/disk (red), symmetry-broken ring/disk (green) at normal incidence, and ring (dotted light gray) at grazing incidence [106]. (F, H, K) Logarithmic electric field enhancement colormaps at the indicated resonances in parts E, G, and J [106]. The range for each figure is from 1 up to the maximum enhancement (white number).

are, respectively, the antibonding and the bonding modes resulted from the first-order longitudinal mode of the nanorod hybridized with the x-polarized electric dipole mode of the V-shaped nanoantenna. Also, V_1 resonance is almost the same as the fundamental y-polarized electric dipole mode of the V-shaped nanoantenna coupled weakly to the nanorod electric dipole mode. As shown in Figure 4B–D, all of these three modes correspond to an electric field enhancement in the gap ensuring their spatial overlap.

An important subtype of plasmonic dimer nanostructures is core-shell ring-disk nanostructure. Plasmonic modes of a cylindrical metallic ring (shell) can be regarded as a result of hybridization between the plasmonic modes of a metallic cylinder and those of a metallic cylindrical void [115]. Yet, not every two modes can hybridize with each other. Because of the selection rule imposed by the system circular symmetry, only the modes that have the same multipolar order are nonorthogonal and can hybridize with each other [106, 118]. Also, thickness of the shell is the main factor determining the strength of hybridization such that thinner shells lead to stronger hybridizations. Please note that unlike split-ring resonators, ring systems do not support any magnetic plasmonic mode. Figure 4E shows the extinction cross section spectra of a gold ring with $D_{\text{out}} = 350$ nm, $D_{\text{in}} = 200$ nm, and thickness of 50 nm [scanning electron microscopy (SEM) image is shown in the inset] [106]. It can be seen that while the ring shows a series of multipolar (dipole, quadrupole, and octupole) modes under the oblique incidence (dotted light gray curve), only the dipole mode has been excited for the case of the normal incidence illumination (solid dark gray curve). The reason is that because of symmetry effect, quadrupole and octupole modes are not allowed to be excited for this case. The corresponding charge distributions for the multipolar modes are shown in the inset. Electric field amplitude enhancements corresponding to each of these modes for the oblique incidence case are shown in Figure 4F. It is seen that for all three modes, we get a small electric field enhancement near the outer and inner walls of the ring. This reveals that, with this illumination condition, the ring system acts as a multiresonant system with partial spatial mode overlap. On the contrary, it does not show a multiresonant behavior under the normal incidence illumination.

The efficiency of the ring system (in terms of its electric field enhancement factors) can be increased by putting a disk at its center (Figure 4G). Here, the disk diameter is chosen to be $D_{\text{disk}} = 150$ nm (SEM is shown in the inset). Also, the black, the grey, and the red curves represent the disk, the ring, and the ring/disk systems extinction spectra under normal illumination, respectively. In such case, the ring and the disk plasmonic modes hybridize with each other. Again, because of circular symmetry, only the modes with the same multipolar order can hybridize. Specifically, the electric dipole mode of the disk (shown in the inset) off-resonantly hybridizes with the bonding and antibonding electric dipolar modes of the ring, giving rise to a superradiant (high-energy) hybrid mode and a subradiant (low-energy) one for which the charge distributions are shown in Figure 4G inset. Figure 4H depicts

the electric field amplitude enhancements for the disk electric dipole mode and the two concentric ring/disk system modes. It is seen that the maximum enhancement is 12 and 22 for the ring/disk superradiant and subradiant modes, respectively. These values are higher compared with the maximum enhancements in both of the single ring and single disk systems electric dipole modes, which have the enhancement factors of 9 and 10, respectively. Also, it is evident that both modes give the maximum enhancements inside the gap ensuring that the ring/disk system modes spatially overlap.

Performance of the ring/disk system can be further improved by breaking the structure symmetry. Such improvement is achieved through making possible the excitation of high-order dark modes through Fano interference with superradiant modes. Because of having long decay lifetimes, these dark modes can store larger electromagnetic energy and thus usually correspond to large field enhancements. A demonstrative example of this argument can be found in Figure 4J. Here, the green curve represents the extinction cross section of a similar ring/disk system as Figure 4G but with its symmetry broken by offsetting the ring and disk centers (gap of 8 nm). In addition, the red and the dotted grey curves correspond to the concentric ring/disk under normal incidence and the ring under oblique incidence angle, respectively. Comparing these curves clearly reflects excitation of the ring high-order modes for the nonconcentric system. In this case, unlike the concentric system, the selection rules allow hybridization of the modes with a different multipolar order leading to each of the ring modes interacting with all of the disk modes. Modes in each of ring and disk systems can also indirectly interact with the modes in the same system. Accordingly, dark high order modes of the ring off-resonantly couple to the superradiant mode because of which they can be excited in this geometry. Interference of these modes with the superradiant mode is the reason for the existence of the observed Fano resonances in the nonconcentric ring/disk system extinction spectra in Figure 4J. Charge distributions related to each of the nonsymmetric system modes are shown in the Figure 4J inset. It is notable that at Fano interference wavelengths, the charge distribution in the disk is not purely dipolar anymore, and instead, it resembles a quadrupolar charge distribution. Such deviation is due to interference of high-order disk modes that get excited through coupling to the superradiant mode. Figure 4K depicts the electric field enhancement colormaps related to each of the non-concentric ring/disk system modes. It is obvious that while the spatial mode overlap is maintained, the enhancements are significantly larger with the maximum

of 100, 36, and 43 for subradiant, quadrupole Fano, and octupole Fano resonances, respectively. Thus, the system performance as a multiresonant system with spatial mode overlap has significantly improved.

Trimers form when three nanoparticles are arranged in the proximity of each other. In this case, the three nanoparticles can be arranged in a linear style or a circular style. Figure 5A shows a linear heterotrimer system composed of three interacting nanorod-shaped aluminum nanoantennas with the respective arm lengths of 50, 50, and 170 nm and the same gap separations of 20 nm [21]. The width and height of the nanoantennas are both 40 nm. In Figure 5A, the dashed green curve represents the enhancement factors of electric field intensity at the center of the right gap, and solid orange line shows that of the left gap. From these curves, it is clear that we have multiple resonances in the field enhancement inside each of the gaps, indicating that the system has spatially overlapped modes. This is also evident in the electric field intensity colormaps of Figure 5B and C, which correspond to $\lambda = 400$ nm and $\lambda = 800$ nm, respectively. The main reasons for the system having multiple resonances are equal size of the two gaps and their proximity (because of rather small arm length of the middle nanoantenna), which allow their corresponding modes to interact and hybridize with each other. Equal size causes the two gap modes to have a high overlap in the spectral domain. Also, spatial proximity causes them to have a high overlap in the spatial domain. Please note that in this example, if the left nanorod has the same length as the right one, the structure will become centrosymmetric. In such centrosymmetric condition, high order modes can become very dark, and the system will lose its

multiresonant behavior. This is the case that happens for the linear trimer structure reported by Wang et al. [128]. In this system, the antibonding magnetic mode does not get excited because it has a zero net electric dipole moment.

In circular trimers, when the electric dipole modes in individual nanoparticles interact in a bonding manner, they can collectively support an oscillating loop current. This causes their fundamental plasmonic mode to have a nonzero magnetic dipole moment. If the nanoparticles (or nanovoids) have similar geometries and also the system is equilateral, the system will become centrosymmetric, as a result of which, net electric dipole moment of this mode reduces to zero and it becomes purely magnetic. Thus, it cannot be excited by the normal incident light [97, 101]. However, if the light illumination is off-normal, it can be excited by coupling to the out-of-plane magnetic field of the incident light. Also, if the centrosymmetry is broken by violating either of the stated conditions, the mode net electric dipole moment will become nonzero, and it can also be excited by normal excitation. Figure 5D shows a plasmonic trimer system composed of three adjacent nanoparticles in an equilateral arrangement [101]. The near-field electric field enhancement factor of the system at the designated gap points P_1 and P_2 is shown in Figure 5E. Here, dashed curves are related to the x-polarized normal incidence condition, and solid curves are related to the x-polarized tangential light illumination (as in Figure 5D). Under normal illumination, only the electric dipole mode with E' symmetry character (left schematic in Figure 5D) gets excited. Accordingly, the field enhancement at both P_1 and P_2 points only shows a single resonance with a Lorentzian line shape. The enhancement factor is much stronger at

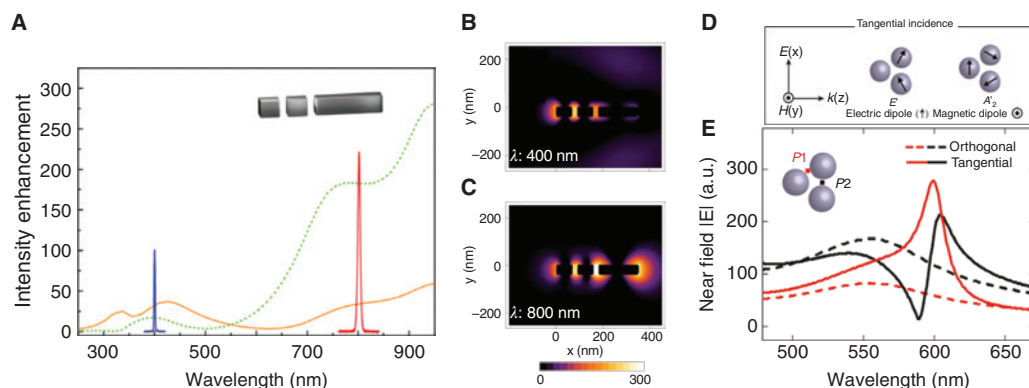


Figure 5: Two examples of multiresonant plasmonic systems based on the optical coupling between localized plasmonic modes in in-plane trimer nanostructures.

(A) Schematic illustration and the spectra of near-field electric field intensity enhancement at two nanogaps in an asymmetric trimer with a linear arrangement [21]; (B, C) The near-field distribution maps of electric field intensity enhancement at (B) $\lambda = 400$ nm and (C) $\lambda = 800$ nm [21]. (D) Schematic illustration and (E) the spectra of electric field at two nanogaps in a trimer system with a circular arrangement under two different polarization conditions of incident light [101].

P_2 , which is inside the electric dipole gap, though. Under tangential illumination, in addition to the electric dipole mode, the magnetic dipole mode with A'_2 symmetry character (right schematic in Figure 5D) can also get excited through coupling to the incident light magnetic field [97]. In this case, as shown in Figure 5E, the electric field at the point P_1 gets prevailed by the dominantly large response of the magnetic dipole mode although it still shows a rather large enhancement factor at the electric dipole mode resonance wavelength. However, at the point P_2 , both of the modes have a comparable field strength. Accordingly, the relatively narrow magnetic dipole optical response interferes with the electric dipole broad response to create a Fano-like resonance behavior with two peaks and a transparency window between them. In the tangential illumination case, the plasmonic trimer system is effectively acting as a multiresonant system with spatial mode overlap that can induce resonant near-field enhancement of electric field over two broad spectra regions at its nanogap positions. It has been demonstrated that through breaking the trimer system symmetry (for example, by making it isosceles instead of equilateral), it is possible to make the magnetic dipole mode net electric dipole moment nonzero, thus having a multiresonant system with spatial mode overlap even for the normal illumination condition [101].

As the number of nanoparticle or nanovoid building blocks further increases (beyond three) in the plasmonic oligomer system, the number of elementary modes in the building blocks as well as their hybridized modes in the composite oligomer system rapidly grows. Despite a more complicated optical response for these high-order oligomers, the physics behind the mode hybridization in them is the same as the simpler dimer or trimer systems. Although these higher-order oligomer systems can support more hybridized modes, many of these modes are not optically active under free space light illumination because their high-order multipolar nature makes them very dark [22, 26, 97, 107, 108, 129, 130].

2.7.2 Core-shell composite nanostructures

Core-shell composite plasmonic nanostructures consist of multiple metal-dielectric core and shell layers. Intuitively, they can be considered as the 3D version of the 2D planar ring/disk plasmonic nanostructures. Similar to a planar plasmonic nanoring, plasmonic modes in a spherical metallic nanoshell originate from the hybridization between elementary plasmonic modes in a metallic sphere and a metallic spherical void. Thickness of the shell determines the strength of hybridization such that a

thinner shell results in stronger hybridization [38, 39, 131]. As schematically shown in Figure 3G, these hybridizations are governed by a selection rule imposed by the spherical system with a rotational symmetry; only modes with the same multipolar order (l) can hybridize with each other [38, 67, 131]. While the bonding mode has a large net electric dipole moment and is a bright mode, the antibonding mode has an electric quadrupolar nature. With a sufficiently large shell thickness, the antibonding mode will also have a net electric dipole moment [67], but this dipole moment will vanish as the shell thickness gets infinitely small [132]. By offsetting the inner shell from the center of the outer shell, we can break the rotational symmetry of the core-shell system and relax the selection rule to allow effective hybridization between the elementary modes in the nanosphere and nanoshells (Figure 3G). Such a lower-symmetry core-shell system is called a “nanoegg,” which can support a larger number of hybridized modes than its concentric counterpart. In such “nanoeggs,” dark and narrow-linewidth hybrid high-order modes can couple to the wideband dipolar modes and thus become bright. Such interaction between dark and bright modes adds several Fano-like resonances to the spectra [67, 131]. As many of these hybrid modes cause a field enhancement in the dielectric core, such core-shell plasmonic nanostructures show a multiresonant optical response with spatially overlapped modes. Another way to reduce the rotational symmetry of core-shell systems is to increase its aspect ratio [66, 131]. In this case, as illustrated in Figure 3F, the degeneracy between the longitudinal and transverse modes gets lifted, and consequently, the number of modes in the system gets doubled under transverse and longitudinal polarization directions. Yet, despite the apparent increasing of the system resonances, this method of symmetry breaking is not very effective to achieve spatial mode overlap between modes with different polarization directions.

By placing a metallic nanosphere close to a plasmonic nanoshell, we are able to create a heterodimer composite system, where the nanosphere plasmonic modes hybridize with those of the nanoshell. Just like a single nanoshell, rotational symmetry in the system causes the hybridization to be only possible between the modes with the same multipolar order [133]. As we have three interacting surfaces in this case, we get three hybrid modes for each multipolar order. Two of these three modes are the bonding and antibonding modes resulted from the hybridization between the nanosphere mode and the nanoshell bonding mode. Also, when the shell is thin, the third hybrid mode is almost the same as the original nanoshell antibonding mode as, because of symmetry effects, it does not hybridize with the nanosphere mode. Accordingly, the number of modes

in a sphere-shell system is $3/2$ that of a single shell structure. Usually, only the lowest order hybrid modes ($l=1$) are bright, and thus, we only get up to three resonances in practice. By breaking the system rotational symmetry, the selection rule for mode hybridization can be relaxed, and many dark high-order modes can become bright through coupling to the bright and wide dipolar modes. Thus, like the nanoeegg case, several Fano-like resonances get added to the system spectra. As many of these modes can induce a large optical field enhancement in the gap, the heterodimer composite nanostructure can serve as a multiresonant plasmonic system with spatial mode overlap. The second case of two nanoparticle core-shell systems is the concentric nanoshell nanostructure [38, 39, 131]. Such system can support four hybridized modes per each of the multipolar orders, which come from the interactions between two elementary modes in the inner nanoshell and the other two in the outer one. In general, the number of modes in a core-shell system can be increased with the total number of metal-dielectric interfaces in the system. Many of these modes are able to provide large optical field enhancements in the dielectric gap layers.

2.7.3 Out-of-plane composite nanostructures

So far, we have talked about the localized-localized coupling strategy based on core-shell and in-plane composite

nanostructures to achieve a multiresonant plasmonic response with spatial mode overlap. In this subsection, we will discuss about out-of-plane composite nanostructures as a multiresonant plasmonic system. A common type of out-of-plane composite plasmonic system is based on multilayered MIM nanostructures consisting of alternative stacks of metal and dielectric (insulator) layers [134–145]. Figure 6A shows the energy diagram for a MIM nanocavity composed of two closely spaced metallic slabs under the normal incidence light illumination with polarization along the x -axis [146–148]. The hybridization of the elementary electric dipole modes in the individual metallic slabs results in a high-energy antibonding mode with an electric dipole nature and a low-energy bonding mode with a magnetic dipole (or electric quadrupolar) nature. Figure 6B shows the simulated scattering and absorption spectra for a single-gap MIM nanocavity. Two major resonances are clear in the far field spectra; the first one is the antibonding electric dipole mode resonance showing a broad peak in the scattering spectra and a very small peak in the absorption spectra around 615 nm, which gets excited by the electric field of the incident light. The second one is the magnetic dipole mode resonance showing narrow peaks in both of the scattering and absorption spectra at the wavelength of $\lambda_{\text{Fund}} = 876$ nm. It is seen that these two modes show a weak Fano-like interference behavior in the scattering spectra. This Fano-like behavior is much stronger if we consider the forward and

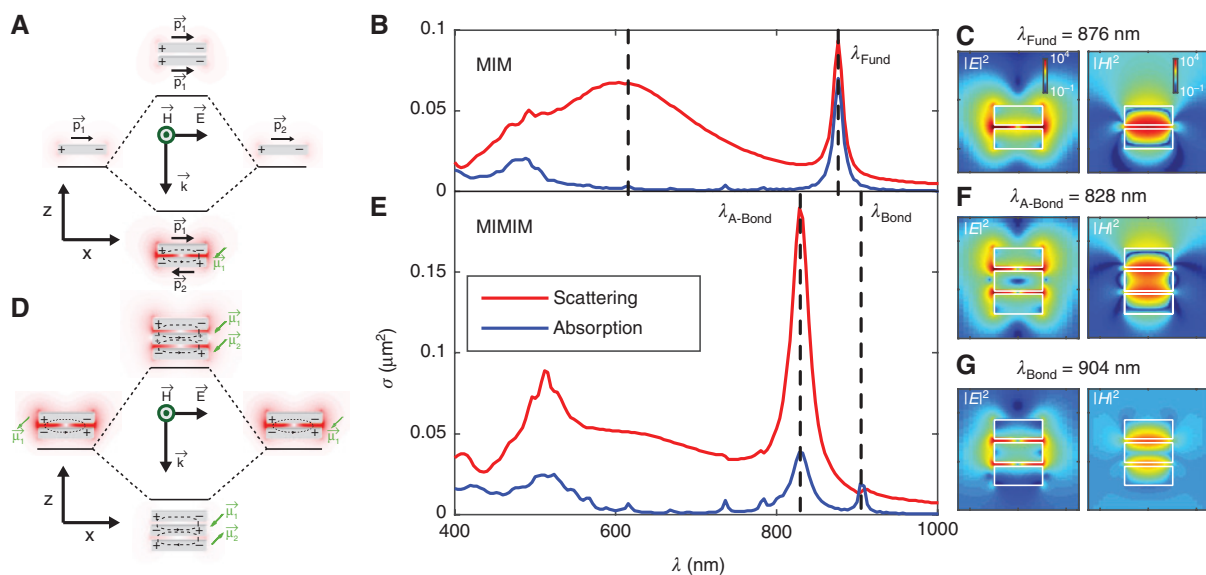


Figure 6: Multiresonant plasmonic systems based on the optical coupling between localized plasmonic modes in out-of-plane composite nanostructures [146, 147].

(A) The energy diagram, (B) the far-field scattering and absorption spectra, and (C) the near-field distribution maps of electric and magnetic field intensities at the magnetic plasmon resonant wavelength for a MIM structure with a single dielectric gap. (D) The energy diagram, (E) the far-field scattering and absorption spectra, and (F–G) the near-field distribution maps of electric and magnetic field intensities at the anti-bonding resonant wavelength (F) and the bonding resonant wavelength (G) for a MIMIM structure with two dielectric gaps.

backward scattering behavior rather than the total one (figure not shown here). The near field colormaps of the electric and magnetic dipole modes in Figure 6C reveal a significant near-field enhancement of electric fields at the gap edge and magnetic fields at the gap center.

Despite providing large electric and magnetic field enhancements by the magnetic dipole mode, such MIM system cannot serve as a multiresonant system with spatial mode overlap. The reason is that the field enhancements are very weak inside the gap at the electric dipole mode resonance wavelength (Figure 6A). The solution to this problem is to create another nanocavity above the first one by switching to a three-metal-layer system as shown in Figure 6D. In this way, the elementary magnetic dipole modes in each of the MIM cavities can hybridize with each other to form new bonding and antibonding modes. For the bonding mode, the two elementary magnetic dipoles are aligned in the opposite directions, which gives this mode a magnetic quadrupolar nature and makes it very dark as revealed in Figure 6E. For the antibonding mode, the elementary magnetic dipoles are aligned in the same direction, which gives this mode a magnetic dipolar nature and makes it brighter as shown in Figure 6E. Weak Fano-like interference between the electric dipole mode, magnetic dipole mode, and magnetic quadrupole mode is also evident in the scattering spectra for this case. Please note that the amount of splitting depends on the strength of magnetic dipoles interaction, which can be easily controlled by the middle metal thickness. The two other important parameters that can be used to control the resonance wavelengths are the gap thicknesses and the metal diameters. Figure 6F and G show a significant near-field enhancement of both bonding and antibonding modes in nanogaps. These observations prove that the two-gap MIM system has spatially overlapped large-field enhancements at two tunable wavelengths.

As we can control the multiresonant optical response of the out-of-plane composite nanostructures by simply engineering out-of-plane geometric parameters of individual building blocks, such designs provide some unique opportunities compared with conventional in-plane plasmonic engineering approaches [143]. First, the vertical arrangement of MIM building blocks results in a nanoscale footprint and a nanoscale volume of such multiresonant devices. Second, by sharing the metal layer between neighboring MIM building blocks in the vertical stack, the out-of-plane arrangement can enable efficient transport of heat or charges between neighboring building blocks triggered by light excitation at multiple different wavelengths. Third, it is much easier to control the out-of-plane geometric parameters at nanoscale (i.e. thin-film

thicknesses) than to define in-plane geometric features by lithography-based processes. Finally, we can incorporate layers of different functional materials (e.g. phase change materials, luminescent materials, and nonlinear optical materials) in different MIM building blocks in the vertical stack, which opens the opportunities to create multiband multifunctional photonics nanodevices.

2.8 Coupling between localized and delocalized modes

In this section, we will review multiresonant plasmonic systems that support hybridized modes formed by the optical coupling between elementary localized modes and delocalized modes in their building blocks. In general, the localized modes can be LSPs associated with metal nanoparticles, while the delocalized modes can be plasmonic Bloch modes in periodic metal-dielectric nanostructures, surface diffraction modes of the grating structure, or SPP modes at the continuous metal-dielectric interface.

2.8.1 Coupling between LSP modes and plasmonic Bloch modes

Large arrays of periodic metal-dielectric nanostructures can support both LSP modes and delocalized plasmonic Bloch modes [149–155]. Compared with a periodically nanotextured continuous metal-insulator interface (e.g. metal nanohole arrays and 1D and 2D metal gratings), arrays of MIM multilayered nanostructures can support a richer set of optical properties because of the interplay between LSP modes and plasmonic Bloch modes at different metal-dielectrics interfaces.

Extensive studies have been carried out to understand the optical response of 1D periodic arrays of MIM nanocavities [149, 151, 153]. Figure 7A illustrates a 1D array of MIM nanocavities that consist of gold nanowire arrays (periodicity of $d_x = 500$ nm) on top of a 20 nm thick silver film with a SiO_2 spacing layer (thickness $L_{\text{sp}} = 20$ nm) illuminated by a TM plane wave at the normal angle [149]. Absorption spectrum (shaded gray area) of the system in part B reveals that the system has two resonances in the wavelength range of interest, each of which correspond to a resonance in the transmission spectra (black solid line) with a Fano line shape. The reason for the emergence of these Fano resonances in the transmittance spectra is the interference of the plasmonic modes scattering in the backward direction, which correspond to discrete resonances with finite linewidth in the spectral

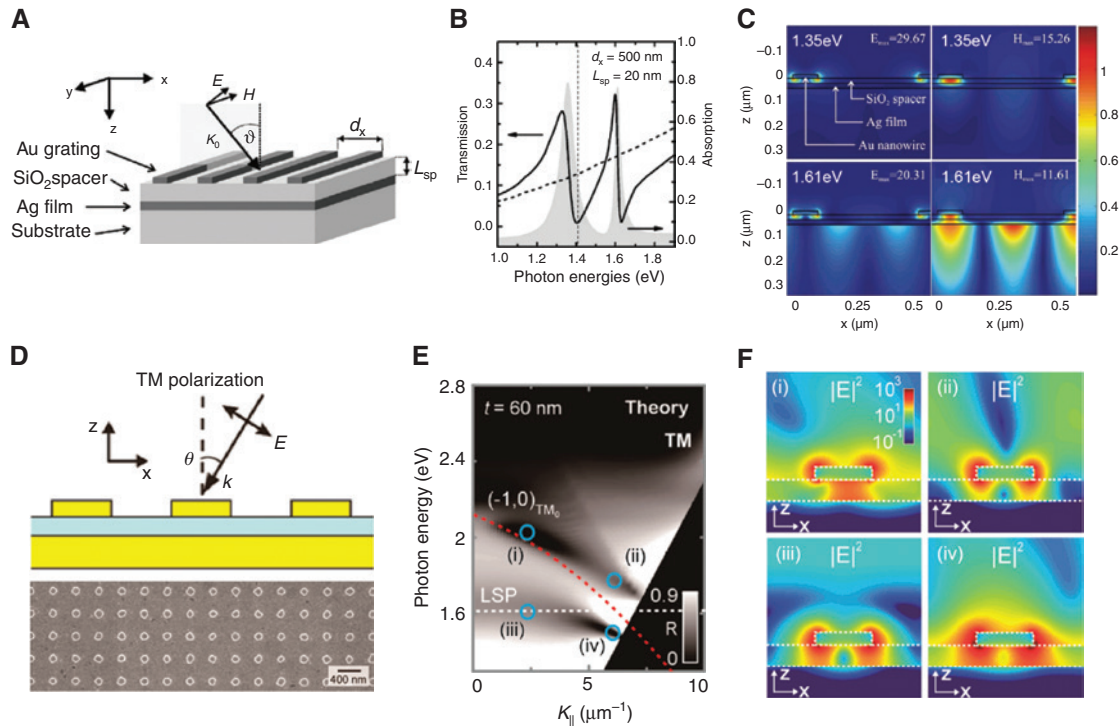


Figure 7: Two examples of multiresonant plasmonic systems based on the optical coupling between localized plasmonic modes and delocalized plasmonic modes.

(A) Schematic illustration of the 1D periodic arrays of MIM nanocavities consisting of 1D periodic array of gold nanowires on an Ag film separated with a SiO₂ dielectric layer [149]. (B) Calculated transmission (solid lines) and absorption spectra (shaded area) for $L_{sp} = 20$ nm, $d_x = 500$ nm with TM polarized normal light incidence that shows two resonant features associated with two hybridized modes [149]. (C) Electric and magnetic field distribution maps for the two hybridized modes at 1.35 and 1.61 eV [149]. (D) Schematic illustration and SEM image of the 2D periodic arrays of MIM nanocavities consisting of a 2D periodic array of gold nanoparticles on an Au film separated with a dielectric layer [150]. (E) Dispersion diagram showing the anti-crossing behavior when the LSP mode is strongly coupled with the Bloch plasmonic mode [150]. (F) Electric field distribution maps for the two branches of modes in the region with no coupling [(i) and (iii)], and with the strong coupling [(ii) and (iv)] [150].

domain, with the normal transmittance through the silver film (dashed curve in Figure 7B) that can be considered as a continuum. From numerical analysis, it gets revealed that the two plasmonic resonances come from the hybridization between elementary localized modes associated with individual nanowires and delocalized plasmonic Bloch modes at periodically modulated metal-dielectric interface. In particular, the localized mode itself is a magnetic dipole mode (it also has an electric quadrupole moment) as a result of out-of-phase coupling between the electric dipole modes in the isolated nanowires and their image dipoles in the silver film. As shown in near field enhancement colormaps of the electric and the magnetic fields (Figure 7C), both of the two modes carry localized and delocalized features of nearfield profiles, indicating their microscopic nature as the hybrid modes from the coupling between localized and delocalized modes. In particular, the localized features of both modes resemble that of the magnetic dipole mode

in a MIM nanocavity, for which, maximum electric field enhancements happen at the gap edges and maximum magnetic field enhancement occurs at the gap center. For both modes, the spatial period of field amplitude at metal-dielectric interface is half of the grating period, which reveals their delocalized nature associated with plasmonic Bloch mode with a grating order of ± 1 at the Brillouin zone edges. As both modes show field enhancements in nanogap regions, such periodic 1D MIM nanostructures can serve as multiresonant plasmonic systems with spatial mode overlap. By altering the nanostructure geometries and the structural periodicity of the system, it is possible to tune and match the resonance wavelengths of elementary localized and delocalized modes to achieve the required spectral mode overlap. By tailoring the SiO₂ spacer layer thicknesses, we can control the coupling strength between elementary localized and delocalized modes and thus modulate the energy splitting between the two hybridized modes.

Despite easy design of 1D periodic MIM nanocavity arrays, their 1D translational symmetry imposes restrictions on the allowed excitation polarizations and directions to achieve multiresonant response. The solution is to use 2D arrays of MIM plasmonic nanocavities that not only avoid such constraints but also provide additional tuning parameters (e.g. lattice symmetry and nanostructure shape) to engineer their optical properties [150, 152, 154, 155]. Figure 7D illustrates an example of such systems [150]. Here, the substrate is a 100 nm gold film and the spacer layer is a polymethylmethacrylate thin film that has a thickness of $t=60$ nm and refractive index of 2.16. Also, the top grating layer has a periodicity of $a_0=400$ nm and is made of gold nanodisks with a diameter of $d=150$ nm and thickness of $h=40$ nm. By angle-resolved reflectance measurements, the band structure of supported optical modes in the 2D MIM plasmonic nanocavity array has been experimentally determined, which also shows a good agreement with the calculation results (Figure 7E) [150]. It is seen that at each $k_{||}$ value, there is a sharp switch between dark and bright regions, which is indicative of Fano-type resonance. The reason for this type of behavior is the interference between the light scattered from the plasmonic modes (which correspond to discrete resonances with finite linewidth) and part of the light reflected from the metal film that can be considered as a continuum in the spectral domain. In addition, the calculated E - k dispersion diagram reveals that the localized plasmon mode and the delocalized Bloch SPP mode can induce an anti-crossing behavior when they are strongly coupled with each other. By comparing the near-field optical properties

of the guided and LSP modes from when there was no coupling to when there was relatively strong hybridization in the anti-crossing region (four different points in Figure 7F), we can see that the hybridization between localized mode and delocalized Bloch mode will result in mixed near-field characters with a very large local field concentration in the gap as well as a 10-fold higher field enhancement surrounding the insulator layer across the entire unit cell [150].

2.8.2 Coupling between LSP modes and diffraction modes

In a plasmonic nanoparticle array system, LSP modes can interact with diffraction surface waves to increase the local field enhancement. Figure 8A depicts a system composed of a single bow-tie nanoantenna surrounded by periodic arrays of metallic disks [156]. The bow-tie antenna aims to provide plasmonic enhancement of optical fields in its gap, while the periodic arrays can further diffractively collect light over a large area and funnel it into the bow-tie antenna at specific wavelengths. To this end, the system is designed such that the broad gap plasmon mode (electric dipole mode) in the bow-tie nanoantenna spectrally overlaps with diffraction modes in the periodic nanodisk arrays (compare blue and red curves in Figure 8B). Furthermore, the nanodisk arrays can be posited in a radial arrangement around the bow-tie antenna to increase the polarization-independent response. Figure 8B reveals that the local

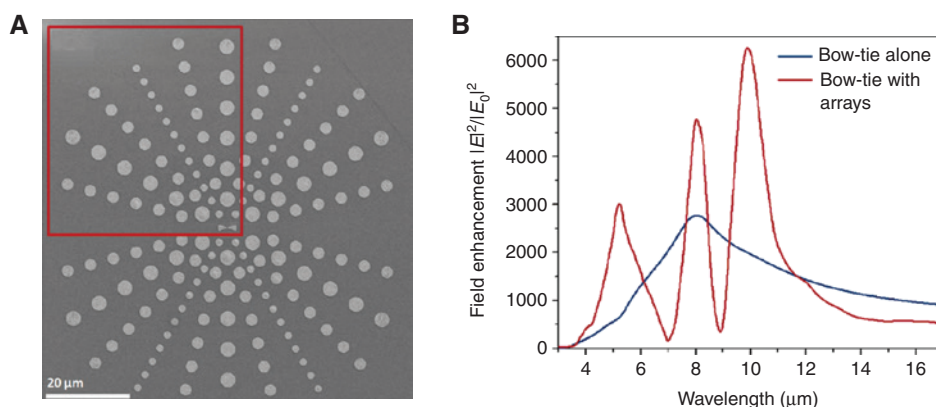


Figure 8: A multiresonant plasmonic system based on the optical coupling between LSP modes and grating diffraction modes [156]. (A) A single bow-tie nanoantenna (two sections of a disk with radius of 2.2 μm, opening angle of 45°, and central gap of 100 nm), surrounded by three periodic arrays (with periodicities of 3.6, 5.7, and 7.2 μm) of metallic disks (with diameters of 1.8, 2.85, and 3.6 μm, respectively). All elements have a thickness of 70 nm and are deposited over a BaF₂ substrate that is transparent in the mid-infrared regime. The bow-tie antenna can couple with the metal particle arrays grating diffraction modes. (B) Simulated electric field intensity enhancement spectrum at the center of the bow-tie antenna at the center of the grating system (red curve) as well as in the isolated state (blue curve).

optical field intensity in the gap can be highly resonantly enhanced at different wavelengths. Under the free-space illumination, the central bow-tie antenna broad gap mode can be excited through two pathways: (1) direct excitation by the incident wave (continuum) and (2) indirect excitation by the diffraction wave from the periodic disk arrays (discrete resonances). Depending on whether two excitation pathways constructively or destructively interfere, we can see subsequent peaks and dips (Fano line shape) in both far-field absorption spectra of the system and near-field enhancement spectra at the gap region of the bow-tie antenna (Figure 8B). By controlling the periodicity of the disk arrays and geometry structure of the bow-tie antenna, we can easily tune the multiresonant response of such system.

2.9 Coupling between delocalized modes

In this section, we briefly discuss the strategy to build multiresonant plasmonic systems through the optical coupling between delocalized plasmonic modes based on rainbow trapping effect in graded grating structures

[157–161]. Figure 9A and B represent a width-graded rainbow trapping 1D plasmonic nanograting structure [161]. We can consider each groove unit as a lossy Fabry-Perot resonator supporting SPP standing waves bouncing back and forth between the two silver side walls. Depending on the groove width, the free-space light only at certain wavelengths can satisfy the phase matching condition and effectively excite SPP standing-wave modes in an individual groove resonator. By putting together large arrays of grooves with different widths side by side, the heterogeneous groove resonator array system can support multiple coupled SPP modes and get excited by the free space light under multiple wavelengths. Moreover, the graded design of the groove widths can result in width-dependent gradient of refractive index for coupled SPP modes in the lateral direction across individual grooves in the system and then cause a build-up of optical fields and energy in the center region with increased refractive index (Figure 9B). Thus, the graded grating system can act as a multiresonant plasmonic system to induce strong local field enhancement at multiple different wavelengths, as shown in Figure 9C–E.

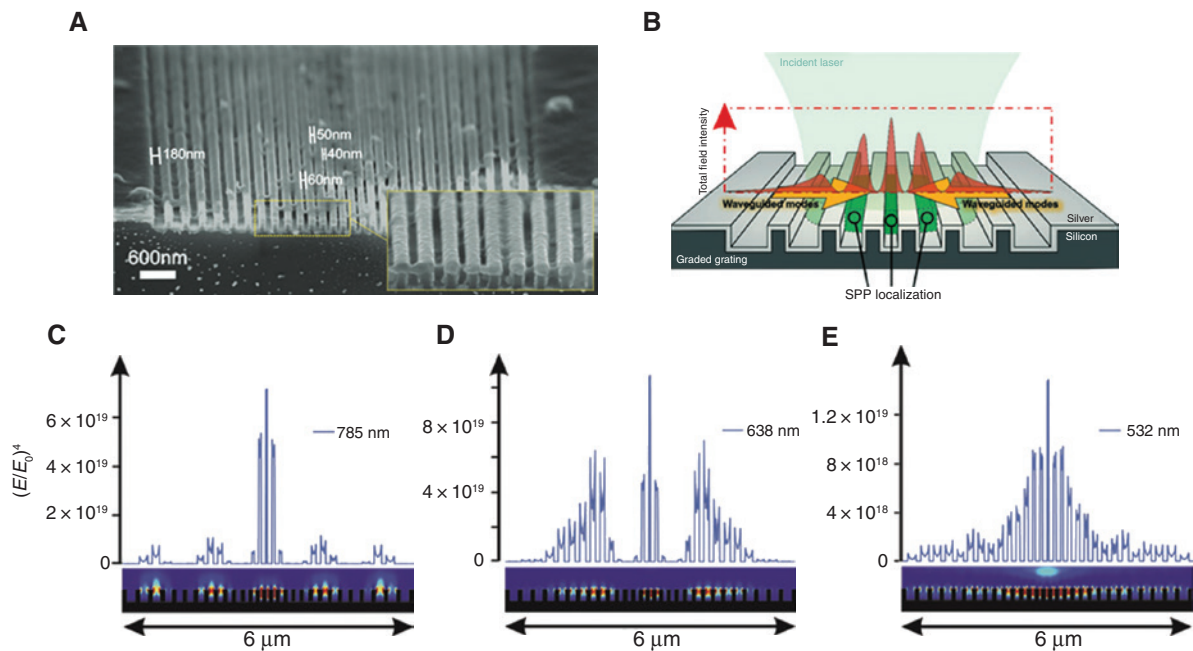


Figure 9: A multiresonant plasmonic system based on the optical coupling between delocalized plasmonic modes [161].

(A) The SEM image of a width-graded rainbow trapping 1D plasmonic nanograting consisting of 29 in-plane MIM rectangular grooves separated from each other by 100 nm thick mesas. All grooves have the same depth of 100 nm. However, their widths increase from 40 nm at the center to 180 nm in both ends in increments of 10 nm. (B) The system schematic diagram. The darker green areas inside the central grooves represent the trapped fields as a result of SPP coupling. Also, the two orange arrows indicate the light guiding in the direction of increasing refractive index toward the center. (C–E) Electric field enhancement factor ($|E/E_0|^4$) patterns in the system for TM-polarized laser excitations at three different wavelengths: (C) 785, (D) 638, and (E) 532 nm.

3 Potential applications enabled by multiresonant plasmonics

Multiresonant plasmonic systems with spatial mode overlap can enhance light-matter interactions at multiple different wavelengths in the same nanolocalized hot spots. Accordingly, they can be uniquely used for two categories of applications either (1) by enabling simultaneous enhancement of both optical excitation and optical emission processes at multiple different wavelengths or by (2) achieving wavelength multiplexed optical multimodalities at nanoscale footprint. In what follows, we elucidate each of these categories in more details.

3.1 Multiresonant plasmonic enhancement of both pumping and emission processes

In optics, frequency conversion has long attracted a great deal of attention spawning a variety of applications in information technology, sensing, and optoelectronics [162–171]. Several frequency conversion optical devices have been demonstrated so far. These optical devices operate on the basis of several nonlinear optical processes, in all of which, some incident (pumped) photons at one or several frequencies are absorbed, and one or several photons with frequencies different from the original ones are emitted.

Depending on their mechanisms, many of these nonlinear optical processes have inherently small efficiencies because of either or both of multiphoton absorption and emission probabilities being low, especially when the pumping rate is low [5, 172–179]. Plasmonic systems have been demonstrated to be a considerable solution to alleviate these limitations and enhance the fast nonlinear optical processes. In general, plasmonic systems could cause two types of enhancements for a nonlinear optical process: excitation enhancement and emission enhancement. Excitation enhancement is achieved through increasing the photon absorption rate via generating large field enhancements at the fundamental wavelengths. Conversely, emission enhancement is obtained by increasing the emission decay rate (Purcell effect) as well as altering the emission quantum yield [174, 179, 180] via increasing the local density of optical states. In the existing literature, most of the plasmonic systems that have been utilized to enhance nonlinear optical processes are single resonant [179]. Such devices have been proven to be very efficient for enhancement of single-photon nonlinear optical processes in which the frequency difference

between the input and output photons is small (like Raman and down-conversion fluorescence) [181–185]. The reason is that plasmonic modes are wide, and thus, both of excitation and emission processes can usually be enhanced by a single mode. However, single-resonant plasmonic devices are usually far less efficient to enhance multiphoton nonlinear optical processes such as sum and difference frequency generation and (multiphoton) UC luminescence. The reason is that in such processes, the frequency difference between the input and output photons is often large, because of which, one mode is not sufficient to enhance both of them simultaneously. The solution to resolve this issue is to use multiresonant plasmonic systems with spatial mode overlap that are capable to enhance every single photon absorption or emission step in a multiphoton nonlinear optical process. In the following subsections, we give short descriptions about parametric nonlinear optical processes and up-conversion luminescence. Also, we discuss the mechanisms through which they can be enhanced using multiresonant plasmonic systems with spatial mode overlap.

3.1.1 Parametric nonlinear optical processes

Electromagnetic waves interact with materials via displacing of their electrons through the electric and magnetic fields. In classic electromagnetics, such interactions are quantified using electric and magnetic susceptibilities, which express the induced electric and magnetic dipole moment (or polarization) densities, respectively [85, 176, 178]. Normally, for a certain material, the electric susceptibility is a constant and does not depend on the field intensity. Yet, when the electric field is large, as can be the case for the lasers, electric susceptibility (or refractive index, equivalently speaking) gets modified according to the field strength; i.e. it becomes nonlinear. Such nonlinearity, which is called a parametric nonlinearity if the susceptibility is a real value [176], can be described by a Taylor series expansion of the polarization density in terms of the electric field. In this regard, linear effects are described by $\chi^{(1)}$, which is a unitless parameter, and quadratic field dependence corresponds to $\chi^{(2)}$, which has the units of m/V and so on. In addition to the classical picture based on high-order electric susceptibilities, quantum mechanical picture, centered on energy and charge conservation, can also be used to describe the parametric nonlinear optical phenomena. In this view, by absorption or emission of photons, electrons gain or lose energy via transitioning through a ladder of virtual states, which are very short-lived and unobservable quantum states. While

the classical description based on the electric susceptibility concept very well serves mathematical analysis purposes, quantum mechanical picture gives a more intuitive view and thus is usually utilized to qualitatively describe the nonlinear optical phenomena [176, 178].

Two major classes of parametric nonlinear optical processes that are highly discussed in the literature are second-order processes, consisting of three-photon sum-frequency generation and three-photon optical parametric amplification (difference frequency generation), and third-order effects, including four-photon sum-frequency process and the four-photon parametric amplification [5, 176, 178, 179]. All of these processes rely on simultaneous absorption of multiple photons, which make their efficiencies very low unless the pumping sources have very high intensities [5, 176–178]. In addition, second-order nonlinear processes are not allowed in the systems that exhibit inversion symmetry, called centrosymmetric systems [5, 176–179]. At macroscale, high nonlinear optical conversion efficiencies are commonly achieved by phase matching in birefringent materials [20, 25, 178]. Yet, typical large dimensions of these materials as well as their dependence upon the incident light polarization prohibit their use to fabricate chip-scale tunable nonlinear optical devices [20].

During the past years, plasmonic systems have been considered a promising solution to address these issues [5, 20–31, 177, 179, 186–196]. There are two major reasons for this consideration: First, as mentioned, plasmonic systems can efficiently enhance excitation or emission processes. Second, the choice of material becomes much more versatile as, although second-order nonlinear optical processes are prohibited in bulk centrosymmetric materials, they are allowed at interfaces because of the broken symmetry. This allows the optical nanoantennas with noncentrosymmetric design to excite second-order optical response from a large range of materials even the centrosymmetric ones.

Commonly, enhancement of parametric nonlinear optical processes is achieved through augmenting of only the excitation rate at the fundamental frequency by single-resonant plasmonic systems [187–196]. Yet, it has been shown that the enhancement factor can be much higher if we also simultaneously augment the emission process [186], a task that can be accomplished only by multiresonant plasmonic systems with spatial mode overlap. Please note that if we have multiple pump wavelengths, the electronic transitions corresponding to each of these wavelengths can be separately enhanced through matching them with the system resonances. These concepts are schematically illustrated in Figure 10A and B, which

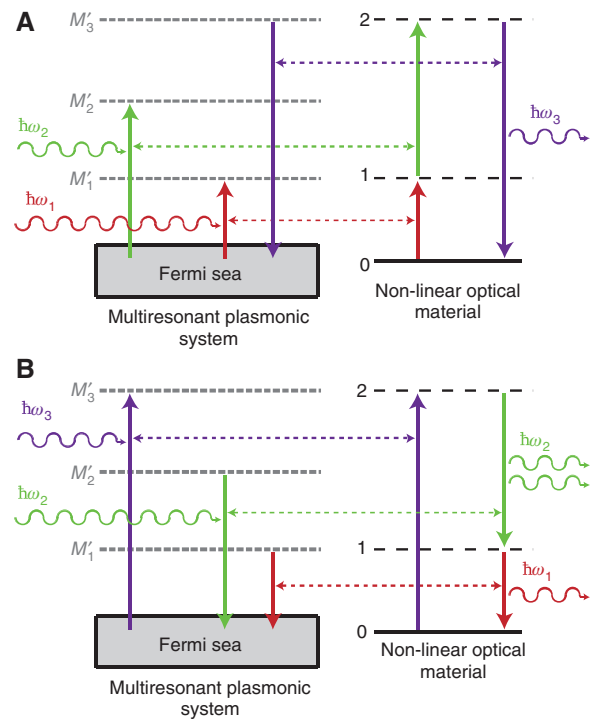


Figure 10: Energy diagram illustration of multiresonant plasmonic enhancement of nanoscale parametric nonlinear optical processes by integrating the nonlinear optical material with a multiresonant plasmonic system with spatial mode overlap. (A) The three-photon sum-frequency process. (B) The three-photon optical parametric amplification process.

represent the energy diagrams regarding the coupling of a multiresonant plasmonic system with a nonlinear material to enhance a three-photon sum-frequency process and a three-photon optical parametric amplification process, respectively. In part A, electronic transitions from the $|0\rangle$ state to the $|1\rangle$ state and from the $|1\rangle$ state to the $|2\rangle$ state are first induced by absorption of pump photons with respective energies of $\hbar\omega_1$ and $\hbar\omega_2$ in the nonlinear optical material. These transitions are augmented through the field enhancements provided by the M_1' and M_2' modes of the multiresonant plasmonic system. After being excited to the $|2\rangle$ state, excited electrons fall down to the ground state ($|0\rangle$) via radiative decay with the photon energy of $\hbar\omega_3$. The radiative decay rate can be modified through the coupling with M_3' mode of the plasmonic system. In part B, by absorbing the pump photons with the energy $\hbar\omega_3$, the system can be excited from the $|0\rangle$ state to the $|2\rangle$ state. This transition is enhanced through the electric field enhancement created by the M_3' plasmonic mode. Then, through stimulated emission of photons with the energy of $\hbar\omega_2$ amplified by the M_2' plasmonic mode, these excited electrons fall down to the $|1\rangle$ electronic state. Finally, via

radiative decay of photons with $\hbar\omega_1$ energy, amplified by M'_1 plasmonic mode, the system goes back to the ground state. Although the two examples discussed here were about second-order (three photon) nonlinear optical processes, similar enhancements by the multiresonant plasmonic systems can be realized for the case of third-order (four photon) processes. During the past recent years, scientists have utilized the idea exhibited in Figure 10A to enhance both second harmonic generation [20–26, 28, 29, 177, 179, 186] and third harmonic generation [30, 31, 179] processes. Feasibility of the idea presented in Figure 10B, i.e. enhancement of optical parametric amplification by multiresonant plasmonic systems, has also recently been demonstrated [27, 179].

3.1.2 UC photoluminescence

UC luminescence is an anti-stokes type photoluminescence process in which low-energy photons in the infrared (IR) or near IR range can be converted into high-energy photons in visible or NIR range [173–175, 197–199]. Unlike parametric nonlinear multiphoton processes mediated by the transition into and from ultrashort-lived virtual states, UC luminescence relies on the excitation and emission transitions between metastable real states. In other words, a parametric nonlinear optical process requires a strict spatiotemporal overlap of multiple photons at different wavelengths for both absorption and radiation and thus is usually induced under pulsed laser excitation with a high optical density. Conversely, the UC luminescence can be generated by a sequential absorption and emission of multiple photons at the same location, which makes it possible to achieve UC luminescence using continuous wave laser excitation with a low optical density [172, 173, 197, 199].

Several mechanisms have so far been identified for multiphoton UC processes [172, 174, 175, 199]. The most elementary of these processes is excited state absorption (ESA). This process, which is illustrated by the energy diagram in Figure 11A, works on the basis of successive absorption of two or more photons by a single ion, called the activator. First, if the resonance conditions are met, the electron gets excited from the ground state to the first metastable excited state (denoted by |1>) by absorption of a pump photon. Then, as this state has a rather long lifetime, the electron remains in it long enough to absorb the second pump photon, leading to its further promotion to a higher excited state (denoted by |2>). Finally, a photon with a higher energy is emitted upon radiative relaxation. Please note that if the energies for the ground and excited states are not equally spaced, more than one

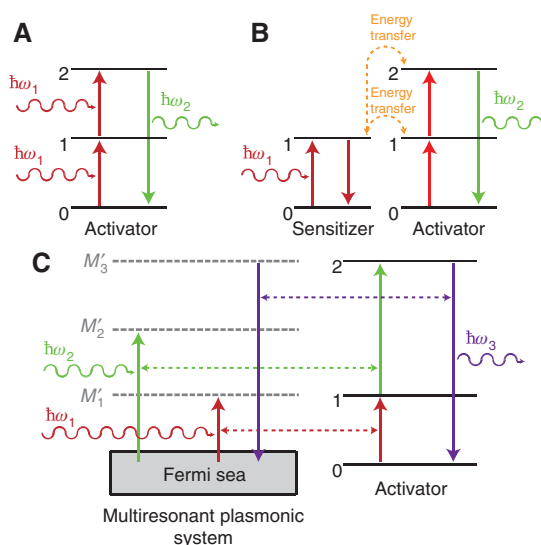


Figure 11: Energy diagram illustration of ESA and ETU UC processes and multiresonant plasmonic enhancement of ESA process by integrating a UC activator ion with a multiresonant plasmonic system with spatial mode overlap. (A) Excited state absorption (ESA) UC process, (B) energy transfer up-conversion (ETU) process, and (C) plasmon enhancement of ESA process by a multiresonant plasmonic system with spatial mode overlap.

pump wavelength is required for the described process. Yet being simple, ESA is a very low efficiency UC mechanism because of low concentration of UC ions dopants as well as their small absorption cross section. In addition, this process has a very low luminescence quantum yield ($<1\%$) [172, 200]. The most common way to enhance the UC efficiency is to use one or more ions, called sensitizers, which have higher absorption cross sections in the neighborhood of the activator ion. The most efficient type of sensitized UC processes is energy transfer UC [172, 174, 175, 199]. In this scenario, which is depicted in Figure 11B, the activator ion excitation rate is enhanced through non-radiative resonance energy transfer from the sensitizer ion. The maximum efficiency happens when the sensitizer electronic transition matches both electronic transitions in the activator as is the case in Figure 11B. Despite their improved efficiencies, sensitized UC processes still suffer from the very low quantum yield [172]. In addition, the efficiency of all UC processes, including energy transfer UC, is highly dependent upon the excitation intensity such that they show much higher efficiencies when the incident power is large [173–175].

During the past years, scientists have demonstrated that plasmonic systems can be used to enhance UC luminescence processes [32–34, 172–174, 197, 198, 201–209]. In general, these systems can improve the efficiency of

sensitized UC processes in three ways: excitation rate enhancement, emission rate enhancement, and energy transfer rate enhancement [173, 174]. Most of previous study on plasmonic enhancement of UC luminescence is focused on single-resonant enhancement of either the emission process [198, 201–203, 208] or the excitation process [197, 204–207]. Yet, the highest enhancement factors can be achieved when both of excitation and emission rates are simultaneously enhanced, which can be achieved by exploiting multiresonant plasmonic systems with spatial mode overlap [32, 34]. If the local field enhancement factors are large for multiple plasmonic modes, it is possible to achieve high UC yields even under the low optical excitation powers. Furthermore, through large enhancement of both emission and excitation rates in activator ions emitters using plasmonic system with spatial mode overlap, it is possible to directly make the ESA process efficient, without the need for any sensitizer [33]. This idea is illustrated in Figure 11C, which shows when an UC activator ion is resonantly coupled to a multiresonant plasmonic system with three spatially overlapped modes (M'_1 , M'_2 , and M'_3 resonant at ω_1 , ω_2 , and ω_3 , respectively), the UC luminescence efficiency can be significantly increased through a simultaneous enhancement of both absorption processes at two fundamental frequencies (ω_1 and ω_2) and the emission process at the emission frequency (ω_3). By avoiding the use of sensitizers for efficient UC luminescence, we will be able to relax the selection of UC activator ions without considering the match of transition energy with limited choices of sensitizer ions. Indeed, it is possible as, by the proper geometric design, one can continuously tune the resonant energies of different modes in multiresonant plasmonic systems to match them with the transitions in the desired activator ion. In this regard, it is notable that while, theoretically speaking, UC can be achieved from most transition metals, lanthanides and actinides, only a few of them have so far been practically reported to give large UC luminescence efficiencies [172].

3.2 Wavelength-multiplexed nanoplasmonic multimodality

Besides multiresonant enhancement of multiphoton nonlinear optical processes and UC luminescence, multiresonant plasmonic systems with spatial mode overlap will open interesting opportunities by enabling wavelength-multiplexed nanoplasmonic multimodality. Excitation of plasmonic modes can strongly enhance

light-matter interactions at nanoscale that can lead to different types of optical processes or effects (Figure 12), including enhanced optical scattering in the far field, enhanced optical fields in the near field [44], nanolocalized photothermal heating [210], or transient generation of hot carriers in metal nanostructures [211]. Up to now, most works on plasmon-enhanced or plasmon-enabled applications focus on utilizing plasmonic effects at a single resonant wavelength range. By exploiting different resonant wavelength bands in multiresonant plasmonic systems with spatial mode overlap, we will be able to combine and merge several different types of plasmonics enabled/enhanced modalities into the same nanoscale devices. Such wavelength-multiplexed multimodal optical nanodevices may find significant applications in fields ranging from biotechnology, to renewable solar energy, and to optical information technology. Potential examples include (1) multimodal biophotonics nanotransducers for combined optical sensing and optical modulation of biochemical and biophysical processes with a subcellular resolution in *in vitro* or *in vivo* biological systems; (2) multimodal broadband light-harvesting substrates that can optically enhance photocatalysis processes in the hot spots and simultaneously achieve *in situ* optical spectroscopy monitoring of photocatalysis processes using another wavelength channel; and (3) wavelength-multiplexed nanoscale all-optical switches or modulators that can use light signals in a group of multiple wavelength bands to control light signals in another group of multiple wavelength bands.

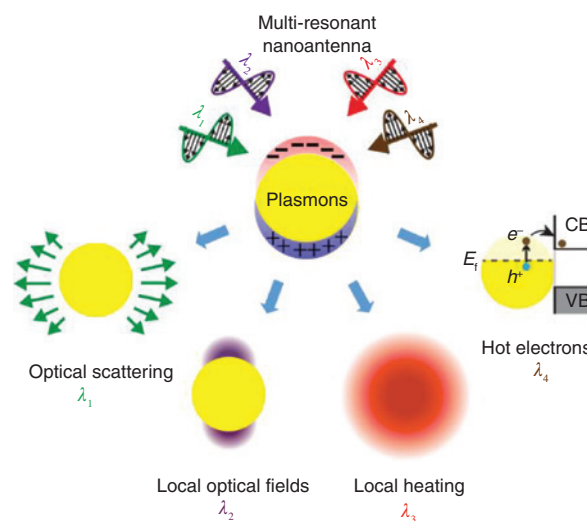


Figure 12: Schematic illustration of the wavelength-multiplexed nanoplasmonic system concept, i.e. merging several different types of plasmonics enabled/enhanced modalities into the same nanoscale device by using different wavelength channels.

4 Conclusions and outlook

This review has summarized the important advances and potential applications in multiresonant plasmonics with spatial mode overlap. First, we introduced the basics of different types of plasmonic modes, the mode hybridization concept, and the geometrical symmetry effects on the optical properties of plasmonic systems. Compared with conventional single-resonant plasmonics targeting at the resonant enhancement of light-matter interactions at a single wavelength band, multiresonant plasmonics requires optical coupling between multiple elementary plasmonic modes to generate multiple new hybridized modes with distinct resonant wavelengths but with spatially overlapped mode profiles. Therefore, a general strategy for the design of multiresonant plasmonic systems is to closely assemble plasmonic building blocks into a composite plasmonic system so that the elementary modes with spatial and spectral overlap in the constitutive building blocks can strongly couple with each other to form new hybridized modes with a controlled energy splitting. In addition, deep understanding of geometrical symmetry effects on the near-field and far-field optical properties of composite plasmonic structures is required to design them in a way that not only provide the required spatial mode overlap but also enable an effective interaction between the plasmonic modes and the free-space light.

Next, we discussed three types of multiresonant plasmonic systems based on the optical coupling between (1) two or more localized modes, (2) localized and delocalized modes, and (3) two or more delocalized modes. Among the three, the multiresonant systems based on the optical coupling between multiple localized modes in closely packed building blocks of metal nanostructure are the most studied type, which can be further classified into three subtypes by the geometric arrangement: (1) in-plane composite nanostructures, (2) core-shell composite nanostructures, and (3) out-of-plane composite nanostructures. A big advantage of the multiresonant systems using the localized-localized mode hybridization is their small footprint and overall volume, suitable for the creation of multiband optical nanodevices for applications such as optical transducers at nano-bio interface with subcellular resolution. Further development in such nano-confined multiresonant plasmonic systems may require a deeper understanding of the microscopic optical coupling mechanism between high-order multipolar LSP modes in building blocks. In contrast to the dipolar interactions between fundamental electric dipolar LSP modes, the coupling between the multipolar LSP modes tends to be more sensitive to effects such as the phase retardation beyond the

quasistatic condition, the geometric symmetry breaking by reducing mode orthogonality, and the magnetic inductive coupling in the near-field.

For multiresonant plasmonic systems using the delocalized-localized mode hybridization, localized modes are typically LSPs associated with metal nanoparticles, while the delocalized modes can be plasmonic Bloch modes in periodic metal-dielectric nanostructures or surface diffraction modes of the grating structure. In particular, 1D and 2D periodic metal-dielectric nanostructures can be exploited as a versatile type of multiresonant plasmonic systems by supporting both localized plasmonic modes in confined metal nanostructures as well as delocalized Bloch plasmonic modes extended over the entire lattice. We can create periodic metal-dielectric nanostructures in a large variety of designs with many degrees of freedom, including multiple in-plane and out-of-plane unit-cell geometry parameters and multiple lattice periodicity and symmetry parameters, and choice of materials. Therefore, we expect that periodic metal-dielectric nanostructures can play a significant role in highly tunable and highly optimized multiresonant plasmonic systems for applications that do not require a device miniaturization for optimal operation. Further development in multiresonant plasmonic systems based on periodic metal-dielectric nanostructures requires a better understanding of the polarization and dispersion effects on the coupling processes between delocalized Bloch plasmonic modes and different types of LSP modes (including the fundamental dipole mode and other high-order multipolar modes).

Finally, we explained that multiresonant plasmonic systems with spatial mode overlap can play a unique role to enable two categories of applications, namely, (1) multiphoton nonlinear optical processes and UC luminescence processes by enabling simultaneous enhancement of both optical excitation and optical emission processes at multiple different wavelengths, and (2) multiband multimodal optical nanodevices by achieving wavelength multiplexed optical multimodalities at nanoscale footprint. For the first category, further advances are required in the following aspects, including (1) the development of a general fabrication strategy for the integration of functional materials (e.g. nonlinear optical materials, rare-earth ion emitter doped materials, or correlated quantum materials) into high-field hot spots in multiresonant plasmonic systems, (2) a deeper understanding of the interplay between plasmonic enhanced emission and plasmonic enhanced excitation processes at multiple wavelength bands before and after the excitation saturation condition, and (3) a deeper understanding of the effects of the transient nanolocalized heating (phonon generation) and

hot-carrier generation processes on parametric nonlinear optical radiation or multiphoton UC luminescence processes. For the second category of wavelength-multiplexed multimodal applications, there is a significant demand to figure out the ways to avoid or decouple the cross-talking of nanoscale plasmonic effects (e.g. enhanced far-field scattering, near-field optical enhancement, nanolocalized heating, and nanolocalized hot carrier generations) between different optical modalities at different operation wavelengths. Possible solutions may include applying the cross-correlation time gating and lock-in amplifier detection techniques.

Acknowledgments: This work was supported by AFOSR Young Investigator Award FA9550-18-1-0328 and NIST grant 70NANB18H20. The authors thank Yuming Zhao and Yizhou Qian for the help on preparing several figures and proofreading the manuscript.

References

- [1] Novotny L, van Hulst N. Antennas for light. *Nat Photonics* 2011;5:83–90.
- [2] Schuller JA, Barnard ES, Cai WS, Jun YC, White JS, Brongersma ML. Plasmonics for extreme light concentration and manipulation. *Nat Mater* 2010;9:193–204.
- [3] Liu Y, Cheng R, Liao L, et al. Plasmon resonance enhanced multicolour photodetection by graphene. *Nat Commun* 2011;2:579.
- [4] Kinkhabwala A, Yu ZF, Fan SH, Avlasevich Y, Mullen K, Moerner WE. Large single-molecule fluorescence enhancements produced by a bowtie nanoantenna. *Nat Photonics* 2009;3:654–7.
- [5] Kauranen M, Zayats AV. Nonlinear plasmonics. *Nat Photonics* 2012;6:737–48.
- [6] Suh JY, Kim CH, Zhou W, et al. Plasmonic Bowtie nanolaser arrays. *Nano Lett* 2012;12:5769–74.
- [7] Celebrano M, Wu X, Baselli M, et al. Mode matching in multiresonant plasmonic nanoantennas for enhanced second harmonic generation. *Nat Nanotechnol* 2015;10:412–7.
- [8] Anker JN, Hall WP, Lyandres O, Shah NC, Zhao J, Van Duyne RP. Biosensing with plasmonic nanosensors. *Nat Mater* 2008;7:442–53.
- [9] Stewart ME, Anderton CR, Thompson LB, et al. Nanostructured plasmonic sensors. *Chem Rev* 2008;108:494–521.
- [10] Ding SY, Yi J, Li J-F, et al. Nanostructure-based plasmon-enhanced Raman spectroscopy for surface analysis of materials. *Nat Rev Mater* 2016;1:16021.
- [11] Lal S, Clare SE, Halas NJ. Nanoshell-enabled photothermal cancer therapy: impending clinical impact. *Accounts Chem Res* 2008;41:1842–51.
- [12] Delcea M, Sternberg N, Yashchenok AM, et al. Nanoplasmonics for dual-molecule release through nanopores in the membrane of red blood cells. *ACS Nano* 2012;6:4169–80.
- [13] Boulais E, Lachaine R, Hatef A, Meunier M. Plasmonics for pulsed-laser cell nanosurgery: fundamentals and applications. *J Photoch Photobio C* 2013;17:26–49.
- [14] Xiong RH, Raemdonck K, Peynshaert K, et al. Comparison of gold nanoparticle mediated photoporation: vapor nanobubbles outperform direct heating for delivering macromolecules in live cells. *ACS Nano* 2014;8:6288–96.
- [15] Carvalho-de-Souza JL, Treger JS, Dang D, Kent SBH, Pepperberg DR, Bezanilla F. Photosensitivity of neurons enabled by cell-targeted gold nanoparticles. *Neuron* 2015;86:207–17.
- [16] Christopher P, Xin HL, Linic S. Visible-light-enhanced catalytic oxidation reactions on plasmonic silver nanostructures. *Nat Chem* 2011;3:467–72.
- [17] Christopher P, Xin HL, Marimuthu A, Linic S. Singular characteristics and unique chemical bond activation mechanisms of photocatalytic reactions on plasmonic nanostructures. *Nat Mater* 2012;11:1044–50.
- [18] Mukherjee S, Libisch F, Large N, et al. Hot electrons do the impossible: plasmon-induced dissociation of H₂ on Au. *Nano Lett* 2013;13:240–7.
- [19] Clavero C. Plasmon-induced hot-electron generation at nanoparticle/metal-oxide interfaces for photovoltaic and photocatalytic devices. *Nat Photonics* 2014;8:95–103.
- [20] Aouani H, Navarro-Cia M, Rahmani M, et al. Multiresonant broadband optical antennas as efficient tunable nanosources of second harmonic light. *Nano Lett* 2012;12:4997–5002.
- [21] Thyagarajan K, Rivier S, Lovera A, Martin OJF. Enhanced second-harmonic generation from double resonant plasmonic antennae. *Opt Express* 2012;20:12860–5.
- [22] Thyagarajan K, Butet J, Martin OJF. Augmenting second harmonic generation using fano resonances in plasmonic systems. *Nano Lett* 2013;13:1847–51.
- [23] Celebrano M, Wu X, Baselli M, et al. Mode matching in multiresonant plasmonic nanoantennas for enhanced second harmonic generation. *Nat Nanotechnol* 2015;10:412–7.
- [24] O'Brien K, Suchowski H, Rho J, et al. Predicting nonlinear properties of metamaterials from the linear response. *Nat Mater* 2015;14:379–83.
- [25] Gennaro SD, Rahmani M, Giannini V, et al. The interplay of symmetry and scattering phase in second harmonic generation from gold nano-antennas. *Nano Lett* 2016;16:5278–85.
- [26] Liu SD, Leong ES, Li GC, et al. Polarization-independent multiple fano resonances in plasmonic nonamers for multimode-matching enhanced multiband second-harmonic generation. *ACS Nano* 2016;10:1442–53.
- [27] Zhang Y, Manjavacas A, Hogan NJ, et al. Toward surface plasmon-enhanced optical parametric amplification (SPOPA) with engineered nanoparticles: a nanoscale tunable infrared source. *Nano Lett* 2016;16:3373–8.
- [28] Metzger B, Hentschel M, Giessen H. Probing the near-field of second-harmonic light around plasmonic nanoantennas. *Nano Lett* 2017;17:1931–7.
- [29] Yang KY, Butet J, Yan C, Bernasconi GD, Martin OJF. Enhancement mechanisms of the second harmonic generation from double resonant aluminum nanostructures. *ACS Photonics* 2017;4:1522–30.
- [30] You JW, You J, Weismann M, Panoiu NC. Double-resonant enhancement of third-harmonic generation in graphene nanostructures. *Philos Trans A Math Phys Eng Sci* 2017;375:20160313.
- [31] You JW, Panoiu NC. Polarization control using passive and active crossed graphene gratings. *Opt Express* 2018;26:1882–94.

- [32] Lee KT, Park JH, Kwon SJ, et al. Simultaneous enhancement of upconversion and downshifting luminescence via plasmonic structure. *Nano Lett* 2015;15:2491–7.
- [33] Liu X, Lei DY. Simultaneous excitation and emission enhancements in upconversion luminescence using plasmonic double-resonant gold nanorods. *Sci Rep* 2015;5:1–13.
- [34] Kang F, He J, Sun T, Bao ZY, Wang F, Lei DY. Plasmonic dual-enhancement and precise color tuning of gold nanorod@SiO₂ coupled core-shell-shell upconversion nanocrystals. *Adv Funct Mater* 2017;27:1–11.
- [35] Zhang X, Chen YL, Liu RS, Tsai DP. Plasmonic photocatalysis. *Rep Prog Phys* 2013;76:046401.
- [36] Cuffe S, Li D, Zhou Y, et al. Dynamic control of light emission faster than the lifetime limit using VO₂ phase-change. *Nat Commun* 2015;6:8636.
- [37] Caprettini V, Messina GC, Dipalo M, Rocca RL, Cerea A, De Angelis F. SERS spectroscopy, electrical recording and intracellular injection in neuronal networks with 3D plasmonic nanoantennas. *Proc SPIE* 2016;9740: 974002.
- [38] Prodan E, Radloff C, Halas NJ, Nordlander P. A hybridization model for the plasmon response of complex nanostructures. *Science* 2003;302:419–22.
- [39] Prodan E, Nordlander P. Plasmon hybridization in spherical nanoparticles. *J Chem Phys* 2004;120:5444–54.
- [40] Zayats AV, Smolyaninov II, Maradudin AA. Nano-optics of surface plasmon polaritons. *Phys Rep* 2005;408:131–314.
- [41] Sönnichsen C. Plasmons in metal nanostructures. München, Ludwig-Maximilians-Universität, 2001.
- [42] Liu H, Lalanne P. Microscopic theory of the extraordinary optical transmission. *Nature* 2008;452:728–31.
- [43] Zhou W, Hua Y, Huntington MD, Odom TW. Delocalized lattice plasmon resonances show dispersive quality factors. *J Phys Chem Lett* 2012;3:1381–5.
- [44] Maier SA. Plasmonics: fundamentals and applications. NY, USA, Springer Science & Business Media, 2007.
- [45] Barnes WL, Dereux A, Ebbesen TW. Surface plasmon subwavelength optics. *Nature* 2003;424:824–30.
- [46] Hutter E, Fendler JH. Exploitation of localized surface plasmon resonance. *Adv Mater* 2004;16:1685–706.
- [47] Wei H, Reyes-Coronado A, Nordlander P, Aizpurua J, Xu HX. Multipolar plasmon resonances in individual Ag nanorice. *ACS Nano* 2010;4:2649–54.
- [48] Schmidt FP, Dittlbacher H, Hohenester U, Hohenau A, Hofer F, Krenn JR. Dark plasmonic breathing modes in silver nanodisks. *Nano Lett* 2012;12:5780–3.
- [49] Joannopoulos JD, Johnson SG, Winn JN, Meade RD. Photonic crystals: molding the flow of light. 2nd ed, Princeton, NJ, Princeton University Press, 2011.
- [50] El-Kady I, Sigalas MM, Biswas R, Ho KM, Soukoulis CM. Metallic photonic crystals at optical wavelengths. *Phys Rev B* 2000;62:15299–302.
- [51] Genet C, Ebbesen TW. Light in tiny holes. *Nature* 2007;445: 39–46.
- [52] Ebbesen TW, Lezec HJ, Ghaemi HF, Thio T, Wolff PA. Extraordinary optical transmission through sub-wavelength hole arrays. *Nature* 1998;391:667–9.
- [53] Vecchi G, Giannini V, Gómez Rivas J. Surface modes in plasmonic crystals induced by diffractive coupling of nanoantennas. *Phys Rev B* 2009;80:201401.
- [54] Meier M, Wokaun A, Liao PF. Enhanced fields on rough surfaces – dipolar interactions among particles of sizes exceeding the Rayleigh limit. *J Opt Soc Am B* 1985;2:931–49.
- [55] Lamprecht B, Schider G, Lechner RT, et al. Metal nanoparticle gratings: influence of dipolar particle interaction on the plasmon resonance. *Phys Rev Lett* 2000;84:4721–4.
- [56] Zhou W, Odom TW. Tunable subradiant lattice plasmons by out-of-plane dipolar interactions. *Nat Nanotechnol* 2011;6:423–7.
- [57] Zou SL, Janel N, Schatz GC. Silver nanoparticle array structures that produce remarkably narrow plasmon lineshapes. *J Phys Chem* 2004;120:10871–5.
- [58] Auguie B, Barnes WL. Collective resonances in gold nanoparticle arrays. *Phys Rev Lett* 2008;101:143902.
- [59] Chu YZ, Schonbrun E, Yang T, Crozier KB. Experimental observation of narrow surface plasmon resonances in gold nanoparticle arrays. *Appl Phys Lett* 2008;93:181108. <https://doi.org/10.1063/1.3012365>.
- [60] Kravets VG, Schedin F, Grigorenko AN. Extremely narrow plasmon resonances based on diffraction coupling of localized plasmons in arrays of metallic nanoparticles. *Phys Rev Lett* 2008;101:087403.
- [61] Vecchi G, Giannini V, Rivas JG. Surface modes in plasmonic crystals induced by diffractive coupling of nanoantennas. *Phys Rev B* 2009;80:201401.
- [62] Limonov MF, Rybin MV, Poddubny AN, Kivshar YS. Fano resonances in photonics. *Nat Photonics* 2017;11:543–54.
- [63] Jain PK, Eustis S, El-Sayed MA. Plasmon coupling in nanorod assemblies: optical absorption, discrete dipole approximation simulation, and exciton-coupling model. *J Phys Chem B* 2006;110:18243–53.
- [64] Hentschel M, Saliba M, Vogelgesang R, Giessen H, Alivisatos AP, Liu N. Transition from isolated to collective modes in plasmonic oligomers. *Nano Lett* 2010;10:2721–6.
- [65] Dionne JA, Sweatlock LA, Atwater HA, Polman A. Plasmon slot waveguides: towards chip-scale propagation with subwavelength-scale localization. *Phys Rev B* 2006;73:1–9.
- [66] Wang H, Brandl DW, Le F, Nordlander P, Halas NJ. Nanorice: a hybrid plasmonic nanostructure. *Nano Lett* 2006;6:827–32.
- [67] Wang H, Wu Y, Lassiter B, et al. Symmetry breaking in individual plasmonic nanoparticles. *Proc Natl Acad Sci USA* 2006;103:10856–60.
- [68] Joe YS, Satanin AM, Kim CS. Classical analogy of Fano resonances. *Phys Scr* 2006;74:259–66.
- [69] Lovera A, Gallinet B, Nordlander P, Martin OJF. Mechanisms of fano resonances in coupled plasmonic systems. *ACS Nano* 2013;7:4527–36.
- [70] Christ A, Ekinci Y, Solak HH, Gippius NA, Tikhodeev SG, Martin OJF. Controlling the Fano interference in a plasmonic lattice. *Phys Rev B* 2007;76:201405.
- [71] Le F, Brandl DW, Urzhumov YA, et al. Metallic nanoparticle arrays: a common substrate for both surface-enhanced Raman scattering and surface-enhanced infrared absorption. *ACS Nano* 2008;2:707–18.
- [72] Liu N, Langguth L, Weiss T, et al. Plasmonic analogue of electromagnetically induced transparency at the Drude damping limit. *Nat Mater* 2009;8:758–62.
- [73] Liu N, Weiss T, Mesch M, et al. Planar metamaterial analogue of electromagnetically induced transparency for plasmonic sensing. *Nano Lett* 2010;10:1103–7.

- [74] Peng B, Ozdemir SK, Chen W, Nori F, Yang L. What is and what is not electromagnetically induced transparency in whispering-gallery microcavities. *Nat Commun* 2014;5:5082.
- [75] Bernal Arango F, Femius Koenderink A. Polarizability tensor retrieval for magnetic and plasmonic antenna design. *New J Phys* 2013;15:073023.
- [76] Rybin MV, Kapitanova P, Filonov DS, et al. Fano resonances in antennas: general control over radiation patterns. *Phys Rev B* 2013;88:1–8.
- [77] Baryshnikova KV, Petrov MI, Babicheva VE, Belov PA. Plasmonic and silicon spherical nanoparticle antireflective coatings. *Sci Rep* 2016;6:22136.
- [78] Luk'yanchuk B, Zheludev NI, Maier SA, et al. The Fano resonance in plasmonic nanostructures and metamaterials. *Nat Mater* 2010;9:707–15.
- [79] Mie GJAP. Articles on the optical characteristics of turbid tubes, especially colloidal metal solutions. *Ann Phys* 1908;25:377–445.
- [80] Aden AL, Kerker M. Scattering of electromagnetic waves from two concentric spheres. *J Appl Phys* 1951;2:1242–6.
- [81] Yee KS. Numerical solution of initial boundary value problems involving Maxwells equations in isotropic media. *IEEE T Antenn Propag* 1966;14:302–7.
- [82] Waterman PC. Symmetry, unitarity, and geometry in electromagnetic scattering. *Phys Rev D* 1971;3:825–39.
- [83] Draine BT, Flatau PJ. Discrete-dipole approximation for scattering calculations. *J Opt Soc Am A* 1994;11:1491–9.
- [84] Volakis JL, Volakis JL, Chatterjee A, Kempel LC. Finite element method for electromagnetics. Piscataway, NJ, Wiley-IEEE Press, 1998.
- [85] Jackson JD. Classical electrodynamics. 3rd ed, NY, USA, Wiley, 1999.
- [86] Mishchenko MI, Travis LD, Lacis AA. Scattering, absorption, and emission of light by small particles. Cambridge, UK, Cambridge University Press, 2002.
- [87] Girard C. Near fields in nanostructures. *Rep Prog Phys* 2005;68:1883–933.
- [88] Khoury CG, Norton SJ, Vo-Dinh T. Plasmonics of 3-D nanoshell dimers using multipole expansion and finite element method. *ACS Nano* 2009;3:2776–88.
- [89] Quinten M. Optical properties of nanoparticle systems: mie and beyond. NY, USA, John Wiley & Sons, 2010.
- [90] Amendola V, Pilot R, Frasconi M, Maragò OM, Iatì MA. Surface plasmon resonance in gold nanoparticles: a review. *J Phys Condens Matter* 2017;29:203002.
- [91] Halas NJ, Lal S, Chang W-S, Link S, Nordlander P. Plasmons in strongly coupled metallic nanostructures. *Chem Rev* 2011;111:3913–61.
- [92] Economou EN. Surface plasmons in thin films. *Phys Rev* 1969;182:539–54.
- [93] Burke JJ, Stegeman GI, Tamir T. Surface-polariton-like waves guided by thin, lossy metal films. *Phys Rev B* 1986;33:5186–201.
- [94] Prade B, Vinet JY, Mysyrowicz A. Guided optical waves in planar heterostructures with negative dielectric constant. *Phys Rev B* 1991;44:13556–72.
- [95] Chen J, Smolyakov GA, Brueck SR, Malloy KJ. Surface plasmon modes of finite, planar, metal-insulator-metal plasmonic waveguides. *Opt Express* 2008;16:14902–9.
- [96] Hamermesh M. Group theory and its application to physical problems. NY, USA, Dover Publications, 2012.
- [97] Brandl DW, Mirin NA, Nordlander P. Plasmon modes of nanosphere trimers and quadrumers. *J Phys Chem B* 2006;110:12302–10.
- [98] Sweatlock LA, Maier SA, Atwater HA, Penninkhof JJ, Polman A. Highly confined electromagnetic fields in arrays of strongly coupled Ag nanoparticles. *Phys Rev B* 2005;71:1–7.
- [99] Liu M, Lee TW, Gray SK, Guyot-Sionnest P, Pelton M. Excitation of dark plasmons in metal nanoparticles by a localized emitter. *Phys Rev Lett* 2009;102:107401.
- [100] Willingham B, Link S. Energy transport in metal nanoparticle chains via sub-radiant plasmon modes. *Opt Express* 2011;19:6450–61.
- [101] Sheikholeslami SN, Garcia-Etxarri A, Dionne JA. Controlling the interplay of electric and magnetic modes via Fano-like plasmon resonances. *Nano Lett* 2011;11:3927–34.
- [102] Nordlander P, Oubre C, Prodan E, Li K, Stockman MI. Plasmon hybridization in nanoparticle dimers. *Nano Lett* 2004;4:899–903.
- [103] Brandl DW, Oubre C, Nordlander P. Plasmon hybridization in nanoshell dimers. *J Chem Phys* 2005;123:24701.
- [104] Hao F, Nordlander P, Burnett MT, Maier SA. Enhanced tunability and linewidth sharpening of plasmon resonances in hybridized metallic ring/disk nanocavities. *Phys Rev B Condens Matter Phys* 2007;76:245417.
- [105] Funston AM, Novo C, Davis TJ, Mulvaney P. Plasmon coupling of gold nanorods at short distances and in different geometries. *Nano Lett* 2009;9:1651–8.
- [106] Sonnefraud Y, Verellen N, Sobhani H, et al. Experimental realization of subradiant, superradiant, and fano resonances in ring/disk plasmonic nanocavities. *ACS Nano* 2010;4:1664–70.
- [107] Barrow SJ, Funston AM, Gomez DE, Davis TJ, Mulvaney P. Surface plasmon resonances in strongly coupled gold nanosphere chains from monomer to hexamer. *Nano Lett* 2011;11:4180–7.
- [108] Dregely D, Hentschel M, Giessen H. Excitation and tuning of higher-order fano resonances in plasmonic oligomer clusters. *ACS Nano* 2011;5:8202–11.
- [109] Yamamoto N, Araya K, García de Abajo FJ. Photon emission from silver particles induced by a high-energy electron beam. *Phys Rev B* 2001;64:205419.
- [110] Aizpurua J, Bryant GW, Richter LJ, García de Abajo FJ, Kelley BK, Mallouk T. Optical properties of coupled metallic nanorods for field-enhanced spectroscopy. *Phys Rev B* 2005;71:235420.
- [111] Hao F, Nordlander P, Sonnefraud Y, Van Dorpe P, Maier SA. Tunability of subradiant dipolar and fano-type plasmon resonances in metallic ring/disk cavities: implications for nanoscale optical sensing. *ACS Nano* 2009;3:643–52.
- [112] Rockstuhl C, Lederer F, Etrich C, Zentgraf T, Kuhl J, Giessen H. On the reinterpretation of resonances in split-ring-resonators at normal incidence. *Opt Express* 2006;14:8827–36.
- [113] Stokes N, Cortie MB, Davis TJ, McDonagh AM. Plasmon resonances in V-shaped gold nanostructures. *Plasmonics* 2011;7:235–43.
- [114] Vercruysse D, Sonnefraud Y, Verellen N, et al. Unidirectional side scattering of light by a single-element nanoantenna. *Nano Lett* 2013;13:3843–9.
- [115] Aizpurua J, Hanarp P, Sutherland DS, Kall M, Bryant GW, García de Abajo FJ. Optical properties of gold nanorings. *Phys Rev Lett* 2003;90:057401.
- [116] Hao E, Schatz GC. Electromagnetic fields around silver nanoparticles and dimers. *J Chem Phys* 2004;120:357–66.

- [117] Guo H, Liu N, Fu L, et al. Resonance hybridization in double split-ring resonator metamaterials. *Opt Express* 2007;15:12095–101.
- [118] Hao F, Sonnefraud Y, Van Dorpe P, Maier SA, Halas NJ, Nordlander P. Symmetry breaking in plasmonic nanocavities: subradiant LSPR sensing and a tunable Fano resonance. *Nano Lett* 2008;8:3983–8.
- [119] Liu N, Kaiser S, Giessen H. Magnetoinductive and electroinductive coupling in plasmonic metamaterial molecules. *Adv Mater* 2008;20:4521–5.
- [120] Dipolar S, Resonances F-tP, Ring M, Cavities D, Sensing NO. Tunability of subradiant dipolar and Fano-type plasmon resonances in metallic ring/disk cavities: implications for nanoscale optical sensing. *ACS Nano* 2009;3:643–52.
- [121] Quintero-Cusguen P, Gutierrez-Alvarez AM. Choreoatetosis as an initial manifestation of HIV-AIDS. *Neurologia* 2009;24:279.
- [122] Aydin K, Pryce IM, Atwater HA. Symmetry breaking and strong coupling in planar optical metamaterials. *Opt Express* 2010;18:13407–17.
- [123] Brown LV, Sobhani H, Lassiter JB, Nordlander P, Halas NJ. Heterodimers: plasmonic properties of mismatched nanoparticle pairs. *ACS Nano* 2010;4:819–32.
- [124] Dong ZG, Liu H, Xu MX, et al. Plasmonically induced transparent magnetic resonance in a metallic metamaterial composed of asymmetric double bars. *Opt Express* 2010;18:18229–34.
- [125] Cetin AE, Altug H. Fano resonant ring/disk plasmonic nanocavities on conducting substrates for advanced biosensing. *ACS Nano* 2012;6:9989–95.
- [126] Dayal G, Chin XY, Soci C, Singh R. High-Q plasmonic fano resonance for multiband surface-enhanced infrared absorption of molecular vibrational sensing. *Adv Opt Mater* 2017;5:1600559.
- [127] Ding P, Liang EJ, Hu WQ, Cai GW, Xue QZ. Tunable plasmonic properties and giant field enhancement in asymmetric double split ring arrays. *Photonic Nanostruct* 2011;9:42–8.
- [128] Wang JQ, Fan CZ, He JN, Ding P, Liang EJ, Xue QZ. Double Fano resonances due to interplay of electric and magnetic plasmon modes in planar plasmonic structure with high sensing sensitivity. *Opt Express* 2013;21:2236–44.
- [129] Lin S, Li M, Dujardin E, Girard C, Mann S. One-dimensional plasmon coupling by facile self-assembly of gold nanoparticles into branched chain networks. *Adv Mater* 2005;17:2553–9.
- [130] Liu K, Xue XZ, Sukhotskiy V, Furlani EP. Optical Fano resonance in self-assembled magnetic-plasmonic nanostructures. *J Phys Chem C* 2016;120:27555–61.
- [131] Wang H, Brandl DW, Nordlander P, Halas NJ. Plasmonic nanostructures: artificial molecules. *Acc Chem Res* 2007;40:53–62.
- [132] Xu X-B, Yi Z, Li X, et al. Discrete dipole approximation simulation of the surface plasmon resonance of core/shell nanostructure and the study of resonance cavity effect. *J Phys Chem Lett* 2012;116:24046–53.
- [133] Hu Y, Noelck SJ, Drezek RA. Symmetry breaking in gold-silica-gold multilayer nanoshells. *ACS Nano* 2010;4:1521–8.
- [134] Johnson PB, Christy RW. Optical constants of the noble metals. *Phys Rev B* 1972;6:4370–9.
- [135] Miyazaki HT, Kurokawa Y. Squeezing visible light waves into a 3-nm-thick and 55-nm-long plasmon cavity. *Phys Rev Lett* 2006;96:097401.
- [136] Bozhevolnyi SI, Sondergaard T. General properties of slow-plasmon resonant nanostructures: nano-antennas and resonators. *Opt Express* 2007;15:10869–77.
- [137] Liu N, Guo HC, Fu LW, Kaiser S, Schweizer H, Giessen H. Plasmon hybridization in stacked cut-wire metamaterials. *Adv Mater* 2007;19:3628–32.
- [138] Liu N, Fu LW, Kaiser S, Schweizer H, Giessen H. Plasmonic building blocks for magnetic molecules in three-dimensional optical metamaterials. *Adv Mater* 2008;20:3859–65.
- [139] Liu N, Guo H, Fu L, Kaiser S, Schweizer H, Giessen H. Three-dimensional photonic metamaterials at optical frequencies. *Nat Mater* 2008;7:31–7.
- [140] Kuttge M, Garcia de Abajo FJ, Polman A. Ultrasmall mode volume plasmonic nanodisk resonators. *Nano Lett* 2010;10:1537–41.
- [141] Yang J, Sauvan C, Jouanin A, Collin S, Pelouard J-L, Lalanne P. Ultrasmall metal-insulator-metal nanoresonators: impact of slow-wave effects on the quality factor. *Opt Express* 2012;20:16880.
- [142] Liu ZQ, Liu G, Fu G, et al. Common metal-dielectric-metal nanocavities for multispectral narrowband light absorption. *Plasmonics* 2016;11:781–6.
- [143] Song J, Zhou W. Multiresonant composite optical nanoantennas by out-of-plane plasmonic engineering. *Nano Lett* 2018;18:4409–16.
- [144] Zhang S, Fan W, Panoiu NC, Malloy KJ, Osgood RM, Brueck SR. Optical negative-index bulk metamaterials consisting of 2D perforated metal-dielectric stacks. *Opt Express* 2006;14:6778–87.
- [145] Dolling G, Wegener M, Linden S. Realization of a three-functional-layer negative-index photonic metamaterial. *Opt Lett* 2007;32:551–3.
- [146] Tali SAS, Zhou W. Magnetic plasmon hybridization in vertically stacked double-gap nanocavities. *Conference on Lasers and Electro-Optics (CLEO)*, Washington, DC, USA, Optical Society of America, 2018, p. FTh4M.5.
- [147] Tali SAS, Zhou W. Multi-resonant optical nanocavities by out-of-plane magnetic plasmon hybridization. *Frontiers in Optics*, Washington, DC, USA, Optical Society of America, 2018, p. JTu3A.53.
- [148] Tali SAS, Zhou W. Magnetic plasmon hybridization in out-of-plane double-gap nanocavities. 2019 (in preparation).
- [149] Christ A, Zentgraf T, Tikhodeev SG, Gippius NA, Kuhl J, Giessen H. Controlling the interaction between localized and delocalized surface plasmon modes: experiment and numerical calculations. *Phys Rev B* 2006;74:155435.
- [150] Zhou W, Suh JY, Hua Y, Odom TW. Hybridization of localized and guided modes in 2D metal-insulator-metal nanocavity arrays. *J Phys Chem C* 2013;117:2541–6.
- [151] Christ A, Zentgraf T, Tikhodeev SG, et al. Interaction between localized and delocalized surface plasmon polariton modes in a metallic photonic crystal. *Phys Status Solidi (B)* 2006;243:2344–8.
- [152] Cesario J, Gonzalez MU, Cheylan S, Barnes WL, Enoch S, Quidant R. Coupling localized and extended plasmons to improve the light extraction through metal films. *Opt Express* 2007;15:10533–9.
- [153] Christ A, Lévêque G, Martin OJ, et al. Near-field-induced tunability of surface plasmon polaritons in composite metallic nanostructures. *J Microsc* 2008;229:344–53.

- [154] Torrado JF, Gonzalez-Diaz JB, Gonzalez MU, Garcia-Martin A, Armelles G. Magneto-optical effects in interacting localized and propagating surface plasmon modes. *Opt Express* 2010;18:15635–42.
- [155] Lodewijks K, Ryken J, Van Roy W, Borghs G, Lagae L, Van Dorpe P. Tuning the Fano resonance between localized and propagating surface plasmon resonances for refractive index sensing applications. *Plasmonics* 2013;8:1379–85.
- [156] Blanchard R, Boriskina SV, Genevet P, et al. Multi-wavelength mid-infrared plasmonic antennas with single nanoscale focal point. *Opt Express* 2011;19:22113–24.
- [157] Tsakmakidis KL, Boardman AD, Hess O. ‘Trapped rainbow’ storage of light in metamaterials. *Nature* 2007;450:397–401.
- [158] Fu Z, Gan Q, Ding YJ, Bartoli FJ. From waveguiding to spatial localization of THz waves within a plasmonic metallic grating. *IEEE J Sel Top Quantum Electron* 2008;14:486–90.
- [159] Gan Q, Fu Z, Ding YJ, Bartoli FJ. Ultrawide-bandwidth slow-light system based on THz plasmonic graded metallic grating structures. *Phys Rev Lett* 2008;100:256803.
- [160] Gan Q, Gao Y, Wagner K, Vezenov D, Ding YJ, Bartoli FJ. Experimental verification of the rainbow trapping effect in adiabatic plasmonic gratings. *Proc Natl Acad Sci USA* 2011;108:5169–73.
- [161] Kazemi-Zanjani N, Shayegannia M, Prinja R, et al. Multiwavelength surface-enhanced Raman spectroscopy using rainbow trapping in width-graded plasmonic gratings. *Adv Opt Mater* 2018;6:1701136.
- [162] Siegel PH. Terahertz technology. *IEEE T Microw Theory* 2002;50:910–28.
- [163] Kajzar F, Lee K-S, Jen AK-Y. *Polymers for photonics applications II*. Berlin, Germany, Springer, 2003.
- [164] Chin SL, Hosseini SA, Liu W, et al. The propagation of powerful femtosecond laser pulses in optical media: physics, applications, and new challenges. *Can J Phys* 2005;83:863–905.
- [165] Ray PC. Size and shape dependent second order nonlinear optical properties of nanomaterials and their application in biological and chemical sensing. *Chem Rev* 2010;736:5332–65.
- [166] Butet J, Russier-Antoine I, Jonin C, Lascoux N, Benichou E, Brevet PF. Sensing with multipolar second harmonic generation from spherical metallic nanoparticles. *Nano Lett* 2012;12:1697–701.
- [167] Butet J, Brevet PF, Martin OJF. Optical second harmonic generation in plasmonic nanostructures: from fundamental principles to advanced applications. *ACS Nano* 2015;9:10545–62.
- [168] Scheps R. Upconversion laser processes. *Prog Quantum Electron* 1996;20:271–358.
- [169] Vetrone F, Naccache R, Zamarrón A, et al. Temperature sensing using fluorescent nanothermometers. *ACS Nano* 2010;4:3254–8.
- [170] Haase M, Schäfer H. Upconverting nanoparticles. *Angew Chem – Int Ed* 2011;50:5808–29.
- [171] Sun LD, Wang YF, Yan CH. Paradigms and challenges for bio-application of rare earth upconversion luminescent nanoparticles: small size and tunable emission/excitation spectra. *Acc Chem Res* 2014;47:1001–9.
- [172] DaCosta MV, Doughan S, Han Y, Krull UJ. Lanthanide upconversion nanoparticles and applications in bioassays and bioimaging: a review. *Anal Chim Acta* 2014;832:1–33.
- [173] Lu D, Cho SK, Ahn S, Brun L, Summers CJ, Park W. Plasmon enhancement mechanism for the upconversion processes in $\text{NaYF}_4:\text{Yb}^{3+}, \text{Er}^{3+}$ nanoparticles: Maxwell versus Förster. *ACS Nano* 2014;8:7780–92.
- [174] Park W, Lu D, Ahn S. Plasmon enhancement of luminescence upconversion. *Chem Soc Rev* 2015;44:2940–62.
- [175] Ye S, Song EH, Zhang QY. Transition metal-involved photon upconversion. *Adv Sci* 2016;3:1600302.
- [176] Boyd RW. *Nonlinear optics*. Amsterdam, Netherlands, Elsevier, 2003.
- [177] Butet J, Brevet PF, Martin OJ. Optical second harmonic generation in plasmonic nanostructures: from fundamental principles to advanced applications. *ACS Nano* 2015;9:10545–62.
- [178] Powers PE, Haus JW. *Fundamentals of nonlinear optics*. FL, USA, CRC Press, 2017.
- [179] Panoiu NC, Sha WEI, Lei DY, Li GC. Nonlinear optics in plasmonic nanostructures. *J Opt* 2018;20:083001.
- [180] Novotny L, Hecht B. *Principles of nano-optics*. 2nd ed, Cambridge, UK, Cambridge University Press, 2012.
- [181] Moskovits M. Surface-enhanced spectroscopy. *Rev Mod Phys* 1985;57:783–826.
- [182] Kneipp K, Wang Y, Kneipp H, et al. Single molecule detection using surface-enhanced Raman scattering (SERS). *Phys Rev Lett* 1997;78:1667–70.
- [183] Kuhn S, Hakanson U, Rogobete L, Sandoghdar V. Enhancement of single-molecule fluorescence using a gold nanoparticle as an optical nanoantenna. *Phys Rev Lett* 2006;97:017402.
- [184] Willets KA, Van Duyne RP. Localized surface plasmon resonance spectroscopy and sensing. *Annu Rev Phys Chem* 2007;58:267–97.
- [185] Kinkhabwala A, Yu Z, Fan S, Avlasevich Y, Müllen K, Moerner WE. Large single-molecule fluorescence enhancements produced by a bowtie nanoantenna. *Nat Photonics* 2009;3:654–7.
- [186] Metzger B, Gui L, Fuchs J, Floess D, Hentschel M, Giessen H. Strong enhancement of second harmonic emission by plasmonic resonances at the second harmonic wavelength. *Nano Lett* 2015;15:3917–22.
- [187] Nahata A, Linke RA, Ishi T, Ohashi K. Enhanced nonlinear optical conversion from a periodically nanostructured metal film. *Opt Lett* 2003;28:423–5.
- [188] Jin R, Jureller JE, Kim HY, Scherer NF. Correlating second harmonic optical responses of single Ag nanoparticles with morphology. *J Am Chem Soc* 2005;127:12482–3.
- [189] Hubert C, Billot L, Adam P-M, et al. Role of surface plasmon in second harmonic generation from gold nanorods. *Appl Phys Lett* 2007;90:181105.
- [190] Pu Y, Grange R, Hsieh CL, Psaltis D. Nonlinear optical properties of core-shell nanocavities for enhanced second-harmonic generation. *Phys Rev Lett* 2010;104:207402.
- [191] Brongersma ML, Cai W, Vasudev AP. Electrically controlled nonlinear generation of light with plasmonics. *Science* 2011;333:1720–3.
- [192] Zhang Y, Grady NK, Ayala-Orozco C, Halas NJ. Three-dimensional nanostructures as highly efficient generators of second harmonic light. *Nano Lett* 2011;11:5519–23.
- [193] Walsh GF, Dal Negro L. Enhanced second harmonic generation by photonic-plasmonic Fano-type coupling in nanoplasmonic arrays. *Nano Lett* 2013;13:3111–7.
- [194] Maier SA, Aouani H, Rahmani M, Navarro-cı M. Third-harmonic-upconversion enhancement from a single semiconductor nanoparticle coupled to a plasmonic antenna. *Nat Nanotechnol* 2014;9:7–11.

- [195] Lehr D, Reinhold J, Thiele I, et al. Enhancing second harmonic generation in gold nanoring resonators filled with lithium niobate. *Nano Lett* 2015;15:1025–30.
- [196] Timpu F, Hendricks NR, Petrov M, et al. Enhanced second-harmonic generation from sequential capillarity-assisted particle assembly of hybrid nanodimers. *Nano Lett* 2017;17:5381–8.
- [197] Paudel HP, Zhong L, Bayat K, et al. Enhancement of near-infrared-to-visible upconversion luminescence using engineered plasmonic gold surfaces. *J Phys Chem C* 2011;115:19028–36.
- [198] Yuan P, Lee YH, Gnanasammandhan MK, Guan Z, Zhang Y, Xu QH. Plasmon enhanced upconversion luminescence of $\text{NaYF}_4\text{:Yb, Er@SiO}_2\text{@Ag}$ core-shell nanocomposites for cell imaging. *Nanoscale* 2012;4:5132–7.
- [199] Zhang F. Photon upconversion nanomaterials. Berlin, Germany, Springer, 2015.
- [200] Chen G, Ohulchanskyy TY, Kachynski A, Agren H, Prasad PN. Intense visible and near-infrared upconversion photoluminescence in colloidal $\text{LiYF}_4\text{:Er(3)+}$ nanocrystals under excitation at 1490 nm. *ACS Nano* 2011;5:4981–6.
- [201] Nakamura T, Fujii M, Usui Y, Aisaka T, Hayashi SJET. Enhancement of upconversion luminescence from Er doped Al_2O_3 films by a thin metal layer. *ECS Trans* 2009;16:87–93.
- [202] Zhang F, Braun GB, Shi Y, et al. Fabrication of $\text{Ag@SiO}_2\text{@Y}_2\text{O}_3\text{:Er}$ nanostructures for bioimaging: tuning of the upconversion fluorescence with silver nanoparticles – Supporting Info. *J Am Chem Soc* 2010;132:2850–1.
- [203] Zhang H, Li Y, Ivanov IA, Qu Y, Huang Y, Duan X. Plasmonic modulation of the upconversion fluorescence in $\text{NaYF}_4\text{:Yb/Tm}$ hexaplate nanocrystals using gold nanoparticles or nanoshells. *Angew Chem Int Ed* 2010;49:2865–8.
- [204] Liu N, Qin W, Qin G, Jiang T, Zhao D. Highly plasmon-enhanced upconversion emissions from $\text{Au@}\beta\text{-NaYF}_4\text{:Yb,Tm}$ hybrid nanostructures. *Chem Commun* 2011;47:7671–3.
- [205] Saboktakin M, Ye X, Chettiar UK, Engheta N, Murray CB, Kagan CR. Plasmonic enhancement of nanophosphor upconversion luminescence in Au nanohole arrays. *ACS Nano* 2013;7:7186–92.
- [206] Feng AL, You ML, Tian L, et al. Distance-dependent plasmon-enhanced fluorescence of upconversion nanoparticles using polyelectrolyte multilayers as tunable spacers. *Sci Rep* 2015;5:1–10.
- [207] Wang YL, Estakhri NM, Johnson A, et al. Tailoring plasmonic enhanced upconversion in single $\text{NaYF}_4\text{:Yb}^{3+}/\text{Er}^{3+}$ nanocrystals. *Sci Rep* 2015;5:1–7.
- [208] He J, Zheng W, Ligmajer F, et al. Plasmonic enhancement and polarization dependence of nonlinear upconversion emissions from single gold nanorod@ $\text{SiO}_2\text{@CaF}_2\text{:Yb}^{3+},\text{Er}^{3+}$ hybrid core-shell-satellite nanostructures. *Light Sci Appl* 2017;6:1–11.
- [209] Uemura T, Furumoto M, Nakano T, et al. Local-plasmon-enhanced up-conversion fluorescence from copper phthalocyanine. *Chem Phys Lett* 2007;448:232–6.
- [210] Pissuwan D, Valenzuela SM, Cortie MB. Therapeutic possibilities of plasmonically heated gold nanoparticles. *Trends Biotechnol* 2006;24:62–7.
- [211] Brongersma ML, Halas NJ, Nordlander P. Plasmon-induced hot carrier science and technology. *Nat Nanotechnol* 2015;10:25–34.